Intel® Model: 18265NGW

FCC ID: PD918265NG

Intel® Model 18265NGW Embedded Inside a notebook brand Dell Model T02J WiGig Subsystem with RFEM 3

RF Exposure Power Density Evaluation and Test Report

September 2017

Revision 1.1

Intel

Notice:

All information provided here is subject to change without notice. Contact your Intel representative to obtain the latest Intel product specifications and roadmaps.

Intel technologies' features and benefits depend on system configuration and may require enabled hardware, software or service activation. Performance varies depending on system configuration. No computer system can be absolutely secure. Check with your system manufacturer or retailer or learn more at [intel.com].

Intel technologies may require enabled hardware, specific software, or services activation. Check with your system manufacturer or retailer.

You may not use or facilitate the use of this document in connection with any infringement or other legal analysis concerning Intel products described herein. You agree to grant Intel a non-exclusive, royalty-free license to any patent claim thereafter drafted which includes subject matter disclosed herein.

No license (express or implied, by estoppel or otherwise) to any intellectual property rights is granted by this document.

The products described may contain design defects or errors known as errata which may cause the product to deviate from published specifications. Current characterized errata are available on request.

Tests document performance of components on a particular test, in specific systems. Differences in hardware, software, or configuration will affect actual performance. Consult other sources of information to evaluate performance as you consider your purchase. For more complete information about performance and benchmark results, visit www.intel.com/benchmarks.

Copies of documents which have an order number and are referenced in this document may be obtained by calling 1-800-548-4725 or visit www.intel.com/design/literature.htm.

Intel, the Intel logo, {List of Intel trademarks} are trademarks of Intel Corporation or its subsidiaries in the U.S. and/or other countries.

*Other names and brands may be claimed as the property of others.

Copyright © 2016 Intel Corporation. All rights reserved.

Contents

1 Document Scope 7
1.1 Introduction 7
1.2 Associated Documents 7
2 Background – WiGig System Operation 8
2.1 System Block Diagram 8
2.2 Beamforming 9
2.3 TX Duty Cycle 10
2.4 Intel 18265NGW module in Dell model T02J 10
3 Beamforming Behavior in Operational Mode 11
3.1 Introduction 11
3.2 Environmental Conditions 11
3.3 Test samples 11
3.4 EUT Features 11
3.5 Test System Description 12
3.5.1 Antenna System and Measurement setup 12
3.6 Test configuration 14
3.7 Test results 17
3.7.1 Case 1: EUT placed horizontally on lap 17
3.7.2 Case 2: EUT placed vertically on lap 19
3.8 Conclusion 21
4 Compliance Assessment 22
Appendix A: Supplemental Numerical Modeling for RF Exposure Power Density Evaluation 23
A.1 Platform Simulation Methodology 23
A.1.1 Assessment considerations 23
A.1.2 Near field and transition-zone field results 23
A.1.3 Simulation tool 24
A.1.4 Finding the near-field, worst-case simulation configuration 26
A.1.5 3D models used in the simulation 32
A.1.6 Antenna feed 36
A.2 Power Density Simulation Results 37
A.2.1 Introduction 37
A.2.2 Upper bound power density values in the evaluation plane 38
A.2.3 Worst-case antenna phases in the evaluation plane 39
A.2.4 Single-Point power density values in the evaluation plane 42
A.2.5 Spatially averaged power density over 1 cm^2 values in the evaluation plane 43
A.2.6 Worst case power density distribution 44
A.2.7 Field and Power Density Distributions for the Six Highest Worst Cases 48
A.2.8 Simultaneous Transmission Evaluation for SAR and Power Density. 55
A.2.9 Conclusion 55
Appendix B: Supplemental Validation of RF Exposure Power Density Simulations Using Near-Field Measurements 56
B.1 Introduction 56
B.2 Probe Characteristics 56
B.3 Total Field and Power Flux Density Reconstruction 57

B.4 Measurement configurations 57
B.5 Measurement results 58
B.6 Conclusion 69

List of Figures

Figure 1 – Intel 18265NGW module system block diagram 9
Figure 2– RFEM 3 Subsets nominal beam directions (horizontal position) 12
Figure 3– RFEM 3 Subsets nominal beam directions (vertical position) 13
Figure 4– Qualitative measurement test setup 14
Figure 5– Qualitative measurement test configuration 15
Figure 6– Height variation for transition zone determination 16
Figure 7– Percentage of subset operation at d=30cm 17
Figure 8– Percentage of subset operation at d=60cm 18
Figure 9– Percentage of subset operation at d=120cm 18
Figure 10– Percentage of subset operation at d=30cm 19
Figure 11– Percentage of subset operation at d=60cm 20
Figure 12– Percentage of subset operation at d=120cm 20
Figure 13 – Illustration of the adaptive mesh technique 24
Figure 14 – The x-y search on the back evaluation plane (blue area) and edge evaluation plane (red area) 26
Figure 15 – Near field worst-case terminology and orientation 27
Figure 16 – Worst-case evaluation plane for Dell model T02J platform 32
Figure 17 – Platform with RFEM 3 location 33
Figure 18 – Platform planes touching the body 34
Figure 19 – Channel 1 upper-bound, single-point power density- subset 1 44
Figure 20 – Channel 1 single-point power density - subset 1 45
Figure 21 – Footprint of single-point power density plane representation 45
Figure 22 – 1-dimensional plots of the power density along x dimension 46
Figure 23 – 1-dimensional plots of the power density along y dimension 46
Figure 24 – Channel 1– spatially averaged power density over 1cm2 - subset 1 47
Figure 25 – SAR and Power Density Distribution for co-located antennas 55

List of Tables

Table 1 – Abbreviations 5
Table 2 – Subsets' sectors 13
Table 3 – Test configuration summary – EUT placed horizontally on lap 16
Table 4 – Test configuration summary – EUT placed vertically on lap 16
Table 5 – Summary of simulation results for RF exposure compliance 22
Table 6 – WiGig channel frequencies 37
Table 7 – Power density simulation configuration and result details 38
Table 8 – Maximum upper bound single point power density [mW/cm^2] 38
Table 9 –Phases configurations for the first worst case for all antenna subsets 40
Table 10 –Phases configurations for the second worst case for all antenna subsets 41
Table 11 – Maximum single point power density [mW/cm^2] 42

Table 12 – Maximum spatially averaged power density over 1cm^2 [mW/cm^2] 43
Table 13 – Worst-case power density – Subset 1..... 47
Table 14 – Highest six worst-case spatially averaged power density 48
Table 15 – Near Field probe Characteristics 56
Table 16 – Test Configuration 57
Table 17 – Case 1#: Simulation Vs. test results @ 2 and 5 mm. 58
Table 18 – Case 2#: Simulation Vs. test results @ 2 and 5 mm. 58
Table 19 – Case 3#: Simulation Vs. test results @ 2 and 5 mm. 59
Table 20 – Case 4#: Simulation Vs. test results @ 2 and 5 mm. 59

List of Abbreviations

Table 1 – Abbreviations

Abbreviation	Definition
Ant	Antenna
Az	Azimuth
BB	Base Band
BF	Beam Forming
BT	Bluetooth
BW	Bandwidth
CPU	Central Processing Unit
El	Elevation
EM	Electro-Magnetic
GHz	Gigahertz
IF	Intermediate Frequency
MAC	Media Access Control
M.2	M2: Formerly known as Next Generation Form Factor (NGFF); used as specification for connectors of the expansion cards mounted on computer
mmWave	Millimeter Wave
PC	Personal Computer
PCIe	Peripheral Component Interconnect Express; a PCI Special Interest Group standard
R&D	Research and Development
RF	Radio Frequency
RFEM 3	Third-generation Radio Front End Module

Abbreviation	Definition
RFIC	Radio Frequency Integrated Circuit
RX	Receive
SKU	Stock Keeping Unit, specific product model version
SoC	System-on-Chip
TDM	Time Division Multiplexing
TPC	Transmit Power Control
T/R SW	Transmit/Receive Switch
TX	Transmit
WiGig	Wireless Gigabit Alliance – the alliance that promoted the 60GHz into 802.11ad standard.

Terms and Definitions

- **Subset:** A predefined group of radiating elements that are excited simultaneously with same amplitude and possibly different phases. There are three Subsets, and each one of them includes between 10 to 12 of the 24 elements of RFEM 3. The Subsets are also called Sub-Arrays.
- **Beamforming Code:** A configuration of phase-shifter values for all of the elements in a specific Subset. The Beamforming Code is used in order to direct the antenna to a desired spatial direction.
- **Sector:** A predefined set of Beamforming Codes, used for automatic selection of the Subset to be used.

1 Document Scope

1.1 Introduction

This report is submitted to support the compliance with the FCC rule located in Title 47 of the Code of Federal Regulations (CFR), parts §2.1093 and §15.255(f), of Intel 18265NGW WiGig module (FCC ID: PD918265NG), including an active antenna array, embedded inside the Dell model T02J.

Per the location of the active antenna array (a.k.a. RFEM 3) in the Dell model T02J platform, the distance between the antenna arrays to the body of an end user, at the closest contact point, will be in the near field.

In order to prove that during typical use the energy goes in most cases away from the human body, several tests of beamforming behavior were performed under different use cases conditions. The results are presented in this document.

These tests are supported by a determination of the near-field power average density performed using an EM simulation supported by a near field measurement. An EM simulation that includes the RFEM 3 transmitter model embedded inside the Dell model T02J is used to determine the worst case configuration and the correspondent near field power density. This worst case power density is considered as a conservative case because the energy is always oriented toward the human body, this latter is also supported by near field measurements. Due to the range of variations and uncertainty introduced by measurement and simulation, the results can only be applied to supplement each other, in conjunction with the beamforming mitigation results, through qualitative comparison and extrapolation to establish compliance at the device surface.

The simulation method, simulation results, and near field measurement results are described in this document. The near field measurement system details are described in document [2]

Chapter 2 provides relevant background on Intel 18265NGW module. Chapter 3 shows the results of the beamforming behavior in operational mode directing the energy away from body. Appendix A describes the simulation methodology to determine the worst case configuration and the power density simulation results, and Appendix B shows the near field measurement results.

1.2 Associated Documents

This Power Density valuation report document as well as the near field measurement document called reference [2] are not confidential; relevant details and explanations that qualify for confidentiality are included separately in the operational description document called reference [1].

[1] "Dell T02J – Theory of Operation Report Revision 1.1".

[2] "170420-01.TR01 - Dell T02J NF-Measurement_TR_Rev.0.1.".

2 Background – WiGig System Operation

2.1 System Block Diagram

The Intel 18265NGW module is a solution for WiGig connectivity for various platforms. The Intel 18265NGW module can be embedded in a conventional clamshell PC as well as in modern 2-in-1 (detachable) platforms and tablet-like platforms (such as the Dell model T02J).

The client solution for Dell T02J includes the 18265NGW WiGig module (FCC ID: PD918265NG) connected to a beam forming antenna array RFEM 3 using one IF coaxial cable.

The WiGig module (FCC ID: PD918265NG) is a PCIe M.2 module consisting of a WiGig BB chip, which implements the WiGig MAC, Modem, BF algorithm, and active antenna array module control, as well as the BB + IF stage circuitry. Intel calls this module Oak Peak. (Note that Oak Peak uses the same WiGig base band silicon as Maple Peak.)

RFEM 3 (10101RRFW) is an active antenna array module, which converts the IF signal to a 60 GHz signal. It also performs the beam forming functionality by phase[1] shifting the RF signal that goes to each antenna. The RFEM 3 is slave to the WiGig BB chip, since all module control and algorithms run on the BB chip.

Intel System-on-Chip (SoC) houses the central processing unit (CPU), which executes applications and provides command and control of the client solution, including all I/O data and addressing.

[1] *Each antenna is excited by an amplitude at a defined phase angle. RFEM 3 feeding circuit has 2 bit phase shifter. Therefore, the phase's values can be 0, 90, 180, or 270 degrees.*

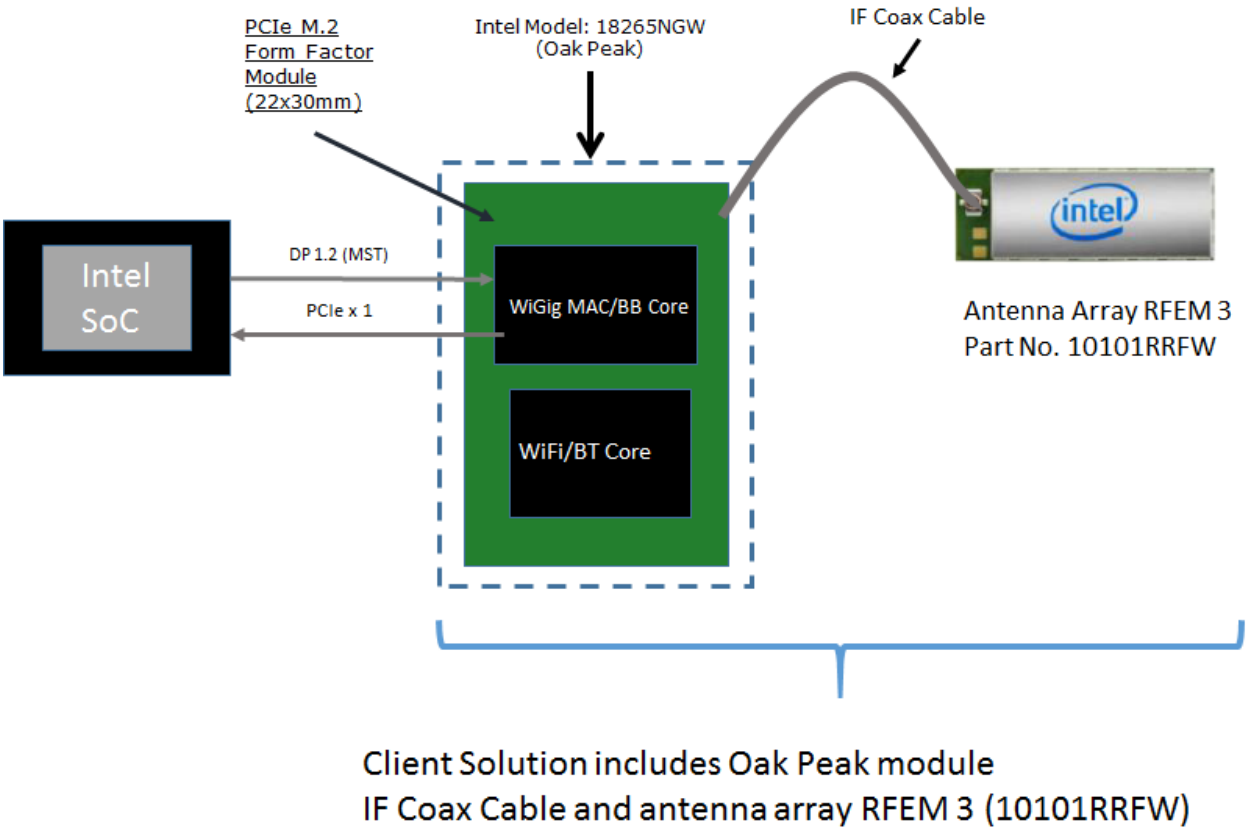

Figure 1 – Intel 18265NGW module system block diagram

Note: Also known by Intel internal project code name "Oak Peak," the above-described WiGig module solution still uses the "Maple Peak" Intel chipset (both MAC/BB chip and radio chip).

2.2 Beamforming

Achieving high-bandwidth communication over 60 GHz channels usually requires directional antennas at the transmitter and receiver sides. In consumer electronics, fixed directional or mechanically-rotated antennas are not practical, and electronically steerable antennas are usually used.

In the Intel 18265NGW module, an electronically-steerable antenna array is used. Beam forming protocol (defined in the IEEE 802.11ad standard) is used to find the right direction for setting both the RX and TX antenna directions.

Due to the RFEM structure, it is not easy to predict the direction and beam forming combination that yields the maximum energy in near field. To find this value, a search over the possible beam forming combination was made and the worst case value was taken. A detailed explanation of this process can be found in Section A.1.4.

2.3 TX Duty Cycle

The WiGig protocol, as defined in ISO/IEC/IEEE 8802-11:2012/Amd.3:2014(E), Clause 21, is packet-based, with time division multiplexing (TDM). The Intel 18265NGW module is configured to guarantee that the TX-Duty-Cycle, defined as the ratio of the duration of all transmissions to the total time, is at most 70% over any 10-second period. This was established by worst-case analysis, as derived from full-system simulation, and verified by measurements.

The limited TX-Duty-Cycle is established based on HW and FW implementation with a measurement interval of ~100 ms (102.4 ms) and 10-second averaging; other details are provided in reference [1]. The 70% duty cycle limitation is guaranteed, independent of user activity, and therefore adheres to the source-based time-averaging definition in Title 47 of the Code of Federal Regulations (CFR) 2.1093(d)(5).

In addition, measurements of the Intel 18265NGW module, configured to obtain maximal TX-Duty-Cycle in a fully loaded system, resulted in an actual maximum TX-Duty-Cycle of 58% over any 10-second period, lower than the upper bound derived from the analysis in this section.

2.4 Intel 18265NGW module in Dell model T02J

Intel produces several HW SKUs (variations) of the Intel 18265NGW module, which target different types of customer platform products.

Dell uses the Intel 18265NGW module inside the Dell model T02J platform. This SKU is characterized by

1. Supporting channels **1+2+3**

2. Reduced power emission, which translates to
   a. Maximum transmit conducted power of **2 dBm** aggregated conducted power at the antenna ports.
   b. Maximum TX duty-cycle of **70%**.

3 Beamforming Behavior in Operational Mode

3.1 Introduction

The goal of this section is to show that during typical use of RFEM 3 inside Dell Model T02J, the energy would go away from the human body. This will be showed by performing several beamforming behaviour tests taking into account different typical heights, distances and EUT orientation.

3.2 Environmental Conditions

At the site where the measurements were performed the following limits were not exceeded during the tests:

Temperature	24ºC ± 1ºC
Humidity	55% ± 10%

3.3 Test samples

Sample	Control #	Description	Model	Serial Number	Date of receipt
#01	170420-01.S01	Tablet PC (with embedded radio module model 18265NGW sn: 3413E8344160)	T02J	4358756100004	2017-03-31
	170420-01.S01	AC Adapter	LA45NM150	CN-0HDCY5-72438-69G-0AB6-A01	2017-03-31
#02	170228-01.S14	Dock Station	WIDOCK-SDS	EZWI51100184	2017-05-11
	170228-01.S14	AC Adapter	NA	NA	2017-05-11

3.4 EUT Features

Brand Name		
Model Name	Client Platform Design Guidelines	
FCC/IC ID	FCC ID: PD918265NG/IC ID: 1000M-18265NG	
Software Version	3.0.41131.1	
Prototype / Production	Production	
Host Identification	T02J series	
Exposure Conditions	Localized free space power density	
Supported Radios	WiGig	60GHz (57.24 – 63.72 GHz)
	802.11b/g/n	2.4GHz (2400.0 – 2483.5 MHz)
	802.11a/n/ac	5.2GHz (5150.0 – 5250.0 MHz) 5.3GHz (5250.0 – 5350.0 MHz) 5.6GHz (5470.0 – 5725.0 MHz) 5.8GHz (5725.0 – 5825.0 MHz)
	Bluetooth	2.4GHz (2400.0 – 2483.5 MHz)
Antenna Information	RFEM3 (10101RRFW)	

Note: RF exposure compliance for 802.11 and Bluetooth capabilities are not addressed in this document neither the associated documents mentioned in section 1.2. The compliance for 82.11 and Bluetooth technologies is addressed in report number "SAR 20170207" dated Feb 8-11, 2017 with FCC ID number PD918265NGU.

3.5 Test System Description

As mentioned in the introduction, the goal of this measurement is to prove that energy goes away from the body when the EUT is at its proximity. The metric that can show this behaviour is the percentage of operation of each subset.

In the tablet mode, the tests are performed with two EUT orientations:

- Case 1: EUT placed horizontally over lap.
- Case 2: EUT placed vertically over lap

The next sections, present the test setup, test configuration and measurement results for the two cases listed above.

3.5.1 Antenna System and Measurement setup

3.5.1.1 Antenna System

Figure 2 illustrates the position of the RFEM 3 antenna when the EUT is placed horizontally (Case 1); this is the case of all test configurations defined in Table 3. The same figure shows the nominal beam direction of each subset. In this case, the tests should prove that subset 2 is operational in the majority of time when the DUT is close to the body in order to direct the beam away.

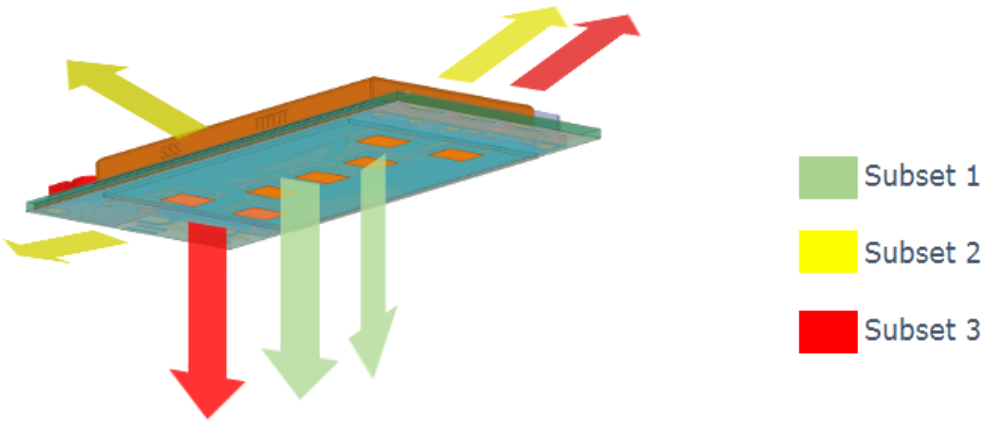

- Subset 2 directed away from leg
- Subset 1 and Subset 3 directed towards leg

Figure 2– RFEM 3 Subsets nominal beam directions (horizontal position)

In the second test case, when the EUT is vertically placed over laps (the tablet edge is touching the body), the tests should prove that subset 1 or subset 3 is operational in the majority of time when the DUT is close to the body in order to direct the beam away.

Figure 3 shows the position of the RFEM 3 antenna when the EUT is vertically placed over laps. The test configurations of this case are mentioned in Table 4.

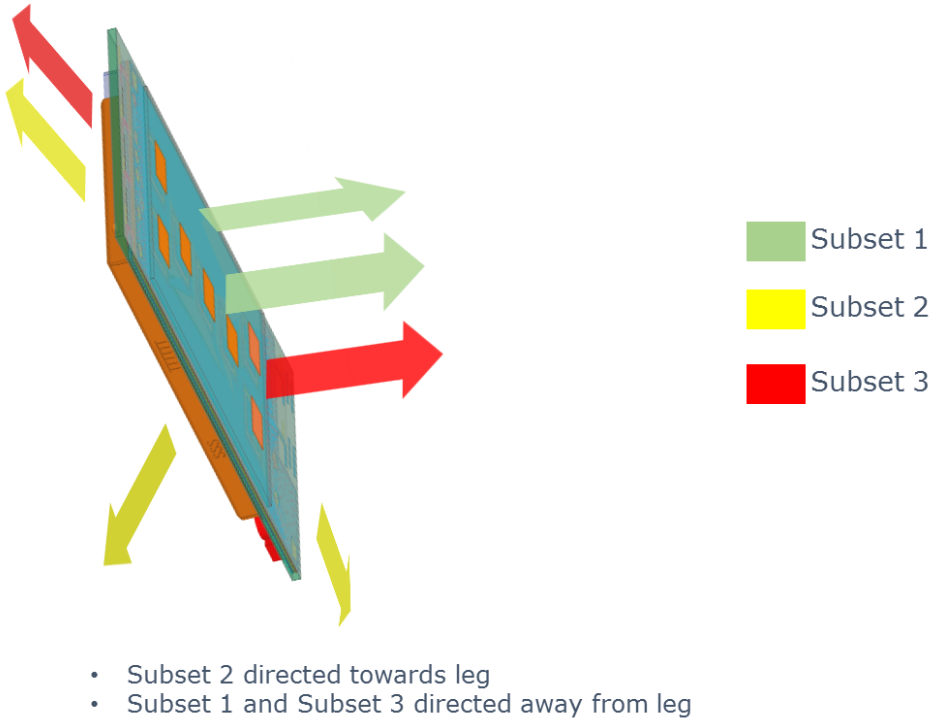

Figure 3– RFEM 3 Subsets nominal beam directions (vertical position)

Note that when a subset is operational, a beamforming code (phases' combination of the subset's elements) among a set of codes (instances) for each subset is realized.

Table 2 illustrates the sectors numbers associated to each subset. The 62 sectors were designed to achieve sufficient coverage in all spatial directions.

Table 2 – Subsets' sectors

Number of Sector															
1	2	3	4	5	6	7	8	9	10	11	12	13	14	15	16
17	18	19	20	21	22	23	24	25	26	27	28	29	30	31	32
33	34	35	36	37	38	39	40	41	42	43	44	45	46	47	48
49	50	51	52	53	54	55	56	57	58	59	60	61	62		
Subset 1								Subset 2						Subset 3	

The second parameter to be studied in these tests is the existence of a transition zone in which a handover from subset to another is observed. This is essential to prove the efficiency of the beamforming algorithm.

3.5.1.2 Measurement Setup

- The dock station is placed on the table with a height of 80 cm above the horizontal office floor.
- The person is holding the EUT horizontally or vertically on his lap.
- Initially, the EUT is touching the person's lap at the evaluation plane as shown in Figure 4. In this case, the dock station and the EUT are at the same height i.e. 80 cm above the horizontal office floor.

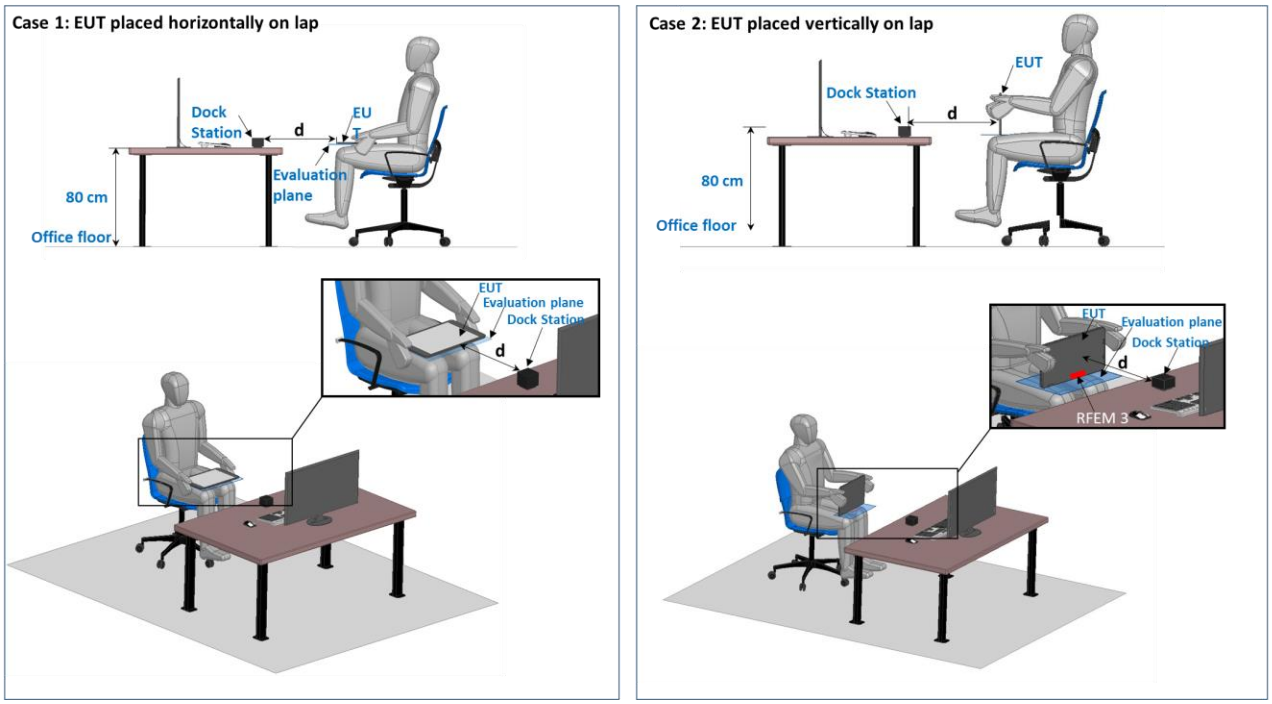

Figure 4– Qualitative measurement test setup

3.6 Test configuration

For each test case, the test configuration is described as follow:

- The EUT and the dock station are set in operational mode and a link condition between the two devices is made using a link software used with Dock and host model T02J in normal operational mode (Wireless Dock Manager, Version 3.0.41131.1).
- The measurement is performed at several distances (d) between the dock station and the EUT i.e. 30 cm, 60 cm, 120 cm. These distances represent three typical use cases and describe three different beam coverages for the operational subsets
- For each distance (d) the test is performed for several heights (h) between the EUT exposure's plane and the person's lap. The height is modified (Figure 6) as described below

  (1) The EUT is raised from the lap position (h=0) until a transition height ($h=h_t$) where a handover between subsets is observed. The handover is a drop of % below 80% for the given subset.

(2) The EUT height is increased until it has passed the transition region in which a handover from a subset to another is observed

(3) The EUT is moved back toward the lap in reverse order until it has passed the lower boundary of the transition region.

- Styrofoam spacers with specific heights are used between the EUT and the person lap's (Figure 5)
- Beam forming triggering in operational mode: when the link is not in maximum MCS[1] (MCS 12) the SW triggers beam forming each 4 seconds.
- In case of abrupt MCS degradation (3 MCS steps) compared to the chosen MCS, or no response from the other side, then there is immediate beam forming triggering. For each EUT position, the measurement time is selected to be sufficient for conditions to stabilize and to record the beamforming code instances. When connection is dropped, the device starts a search phase in which it normally transmits for less than 1ms once per 1 second (<0.1%). Additional transmissions happen only if it finds another device and they start to connect to each other.

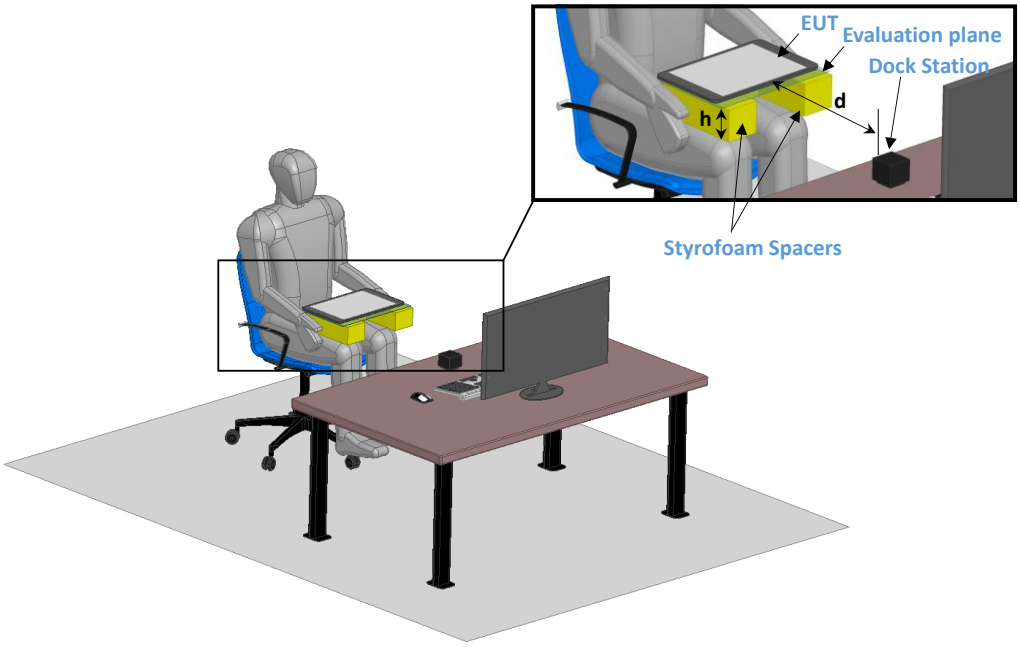

Figure 5– Qualitative measurement test configuration

1: MCS stands for Modulation and Coding Scheme, and it controls the PHY data rate being used per packet. Data MCS ranges between 1 and 12, and the higher the MCS is the higher data rate. The beamforming aims to improve the link conditions. If the MCS is MCS-12, then data-rate is maximal, there's no option to further improve the link, and therefore beamforming is not triggered.

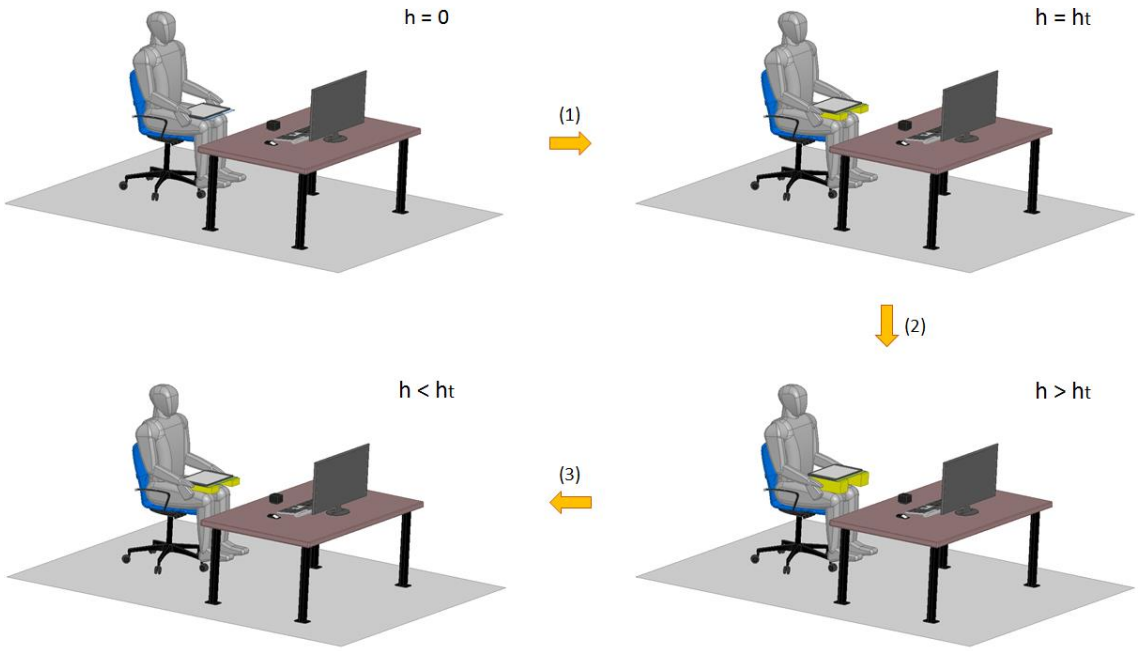

Figure 6– Height variation for transition zone determination

Table 3 and Table 4 summarizes the realized test configuration for the horizontal and vertical measured cases respectively.

Table 3 – Test configuration summary – EUT placed horizontally on lap

Test number	EUT to dock station distance (d)	EUT to person laps distance (h)
1	30 cm	0, 2, 4, 6, 8, 10 and 12 cm
2	60 cm	0, 2, 4, 6, 8, 10, 12, 14 and 16 cm
3	120 cm	0, 2, 4, 6, 8, 10, 12, 14, 16, 18, 20, 22 and 24 cm

Table 4 – Test configuration summary – EUT placed vertically on lap

Test number	EUT to dock station distance (d)	EUT to person laps distance (h)
1	30 cm	0, 2, 4, 8 and 12 cm
2	60 cm	0, 2, 4, 8, 12, 16 cm
3	120 cm	0, 2, 4, 8, 12, 16 and 20 cm

3.7 Test results

3.7.1 Case 1: EUT placed horizontally on lap

Figure 7, Figure 8 and Figure 9 show the test results of the subset operation according to the EUT to lap distance (h), for the three horizontal distances: 30, 60, and 120 cm respectively. The x-axis represents the height above lap while the y-axis represents, for each subset, the percentage of subset operation.

For every measurement point i.e. every h, the total percentage of instances for three subsets is 100%. The 100% of y-axis applies separately for each translation direction. For example, for a given h, if we have 100 beamforming instances, and among these instances we have 90 instances where sub-array 2 is operational , 8 instances where sub-array 3 is operational, 2 instances for sub-array 1, then the percentage of sub-arrays 1, 2 and 3 are 2%, 90% and 8% respectively.

1. **Test 1 results at 30 cm distance**

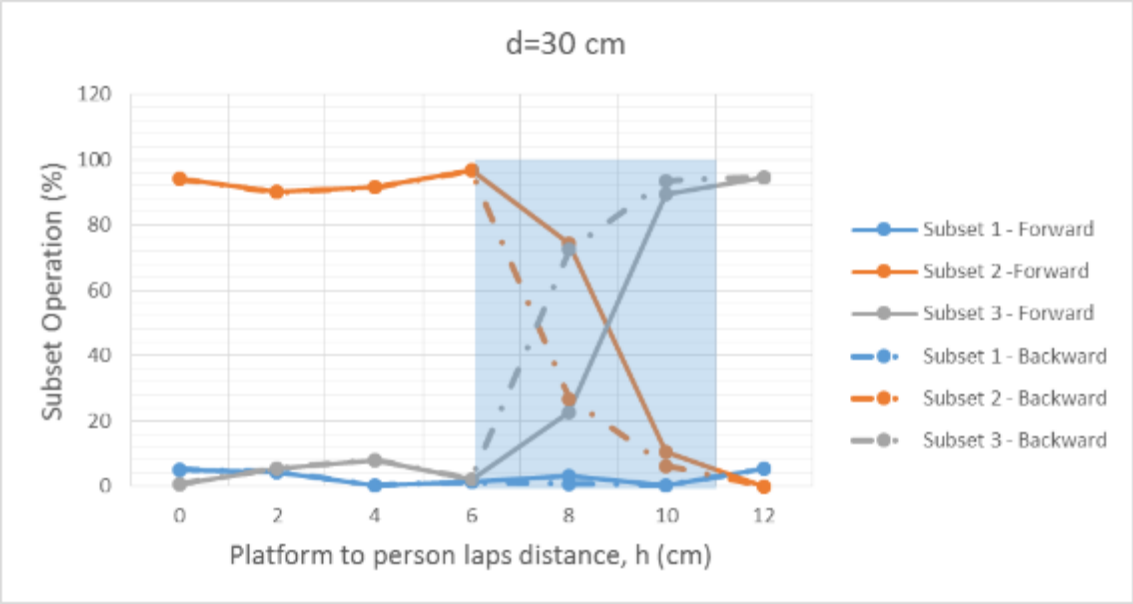

Figure 7– Percentage of subset operation at d=30cm

Figure 7 presents the results of the mitigation test when the user is holding the EUT horizontally on his lap and is placed at a distance of 30 cm from the Docking Station. For h going from 0cm to 12cm subset 2 is 98% operational among the three subsets. A transition zone is observed when h is between 6 and 11cm. This transition zone is a drop of % below 80% for subset 2. For h greater than 11 cm, Subset 3 is always selected. This shows that that the beam steering algorithm behaves in such a manner as to direct the energy away from the body.

2. Test 2 results at 60 cm distance

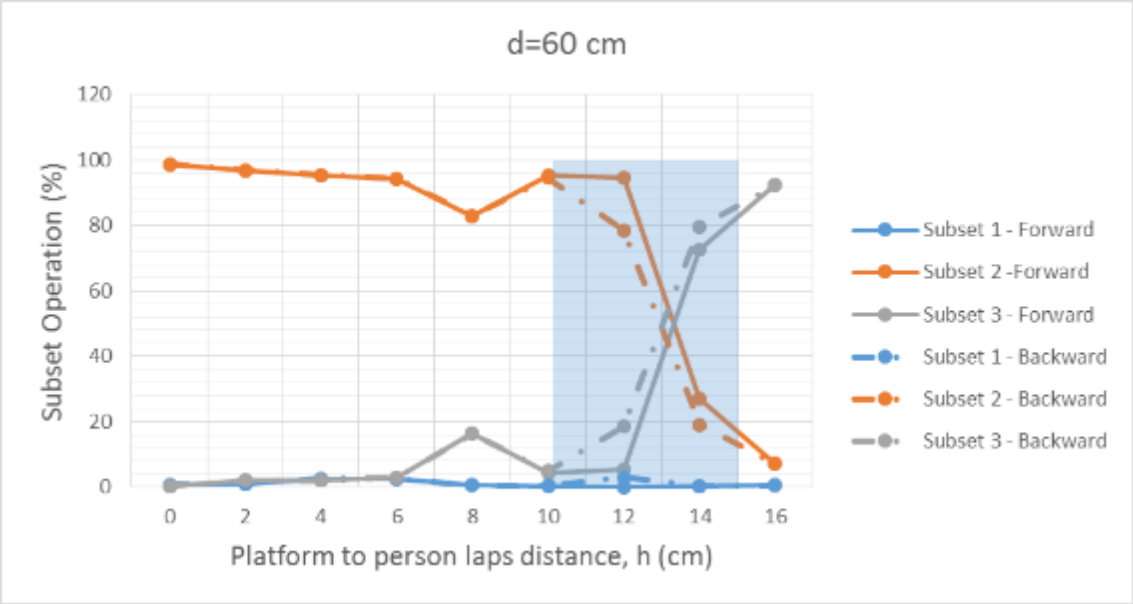

Figure 8– Percentage of subset operation at d=60cm

3. Test 3 results at 120 cm distance

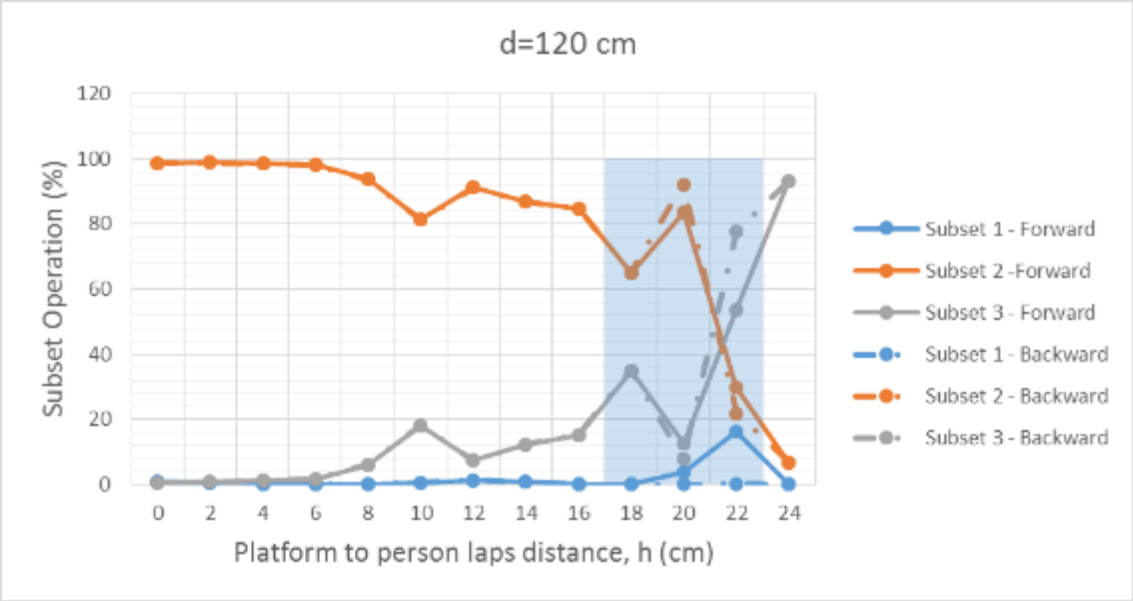

Figure 9– Percentage of subset operation at d=120cm

3.7.2 Case 2: EUT placed vertically on lap

Figure 10, Figure 11 and Figure 12 show the test results of the subset operation according to the EUT to lap distance (h), for the three horizontal distances: 30, 60, and 120 cm respectively. The x-axis represents the height above lap while the y-axis represents, for each subset, the percentage of subset operation.

1. **Test 1 results at 30 cm distance**

Figure 10 presents the test results when the user is holding the EUT vertically on his lap and is placed at a distance of 30 cm from the Docking Station. For h going from 0 cm to 12 cm, the transition region is not observed in this test case since the subset 3 is 100% operational for all heights.

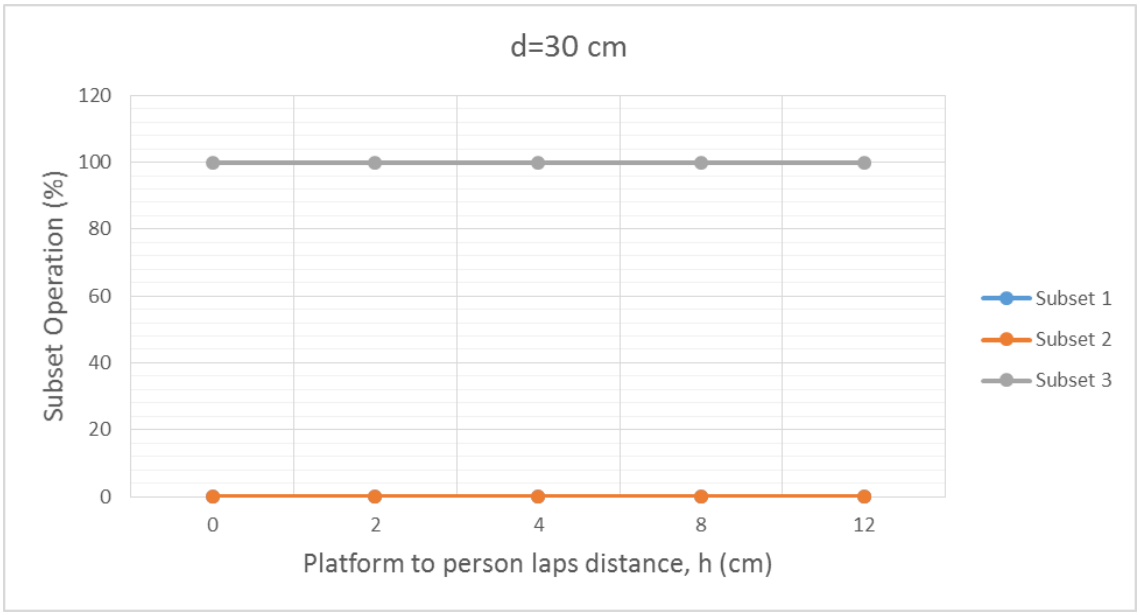

Figure 10– Percentage of subset operation at d=30cm

2. Test 2 results at 60 cm distance

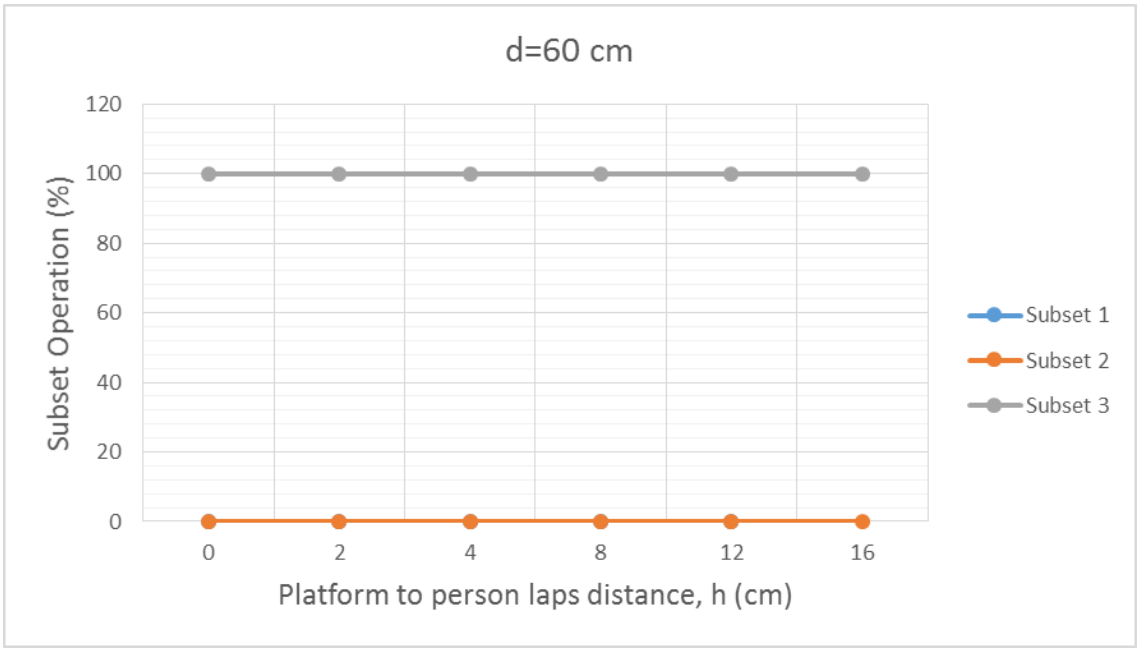

Figure 11– Percentage of subset operation at d=60cm

3. Test 3 results at 120 cm distance

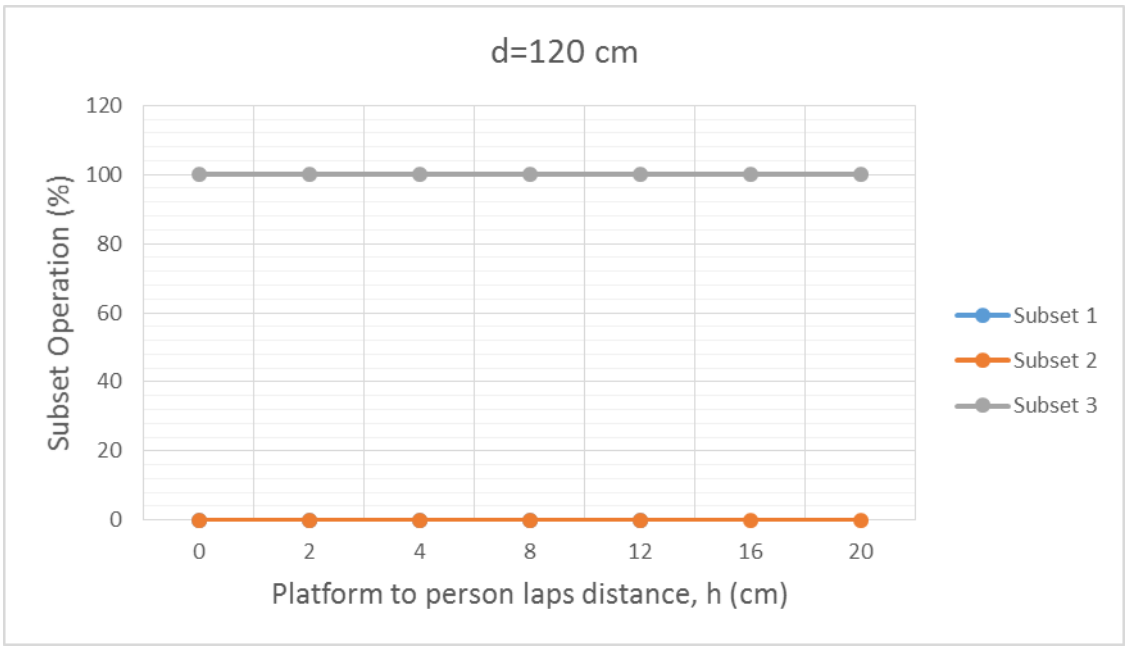

Figure 12– Percentage of subset operation at d=120cm

3.8 Conclusion

For the measured case 1 when the EUT is placed horizontally on lap, the test results presented in section 3.7.1 show that, at each horizontal distance:

- When the EUT is placed close to the lap, subset 2 (orange line) with a beam directed away from the body is operational almost all the time.
- When the EUT is moved forward from the lap, a transition zone is observed (blue area) and a handover from subset 2 to subset 3 is done after this transition zone
- When the EUT is moved back toward the lap in reverse order, the transition zone is observed again and a switch from subset 3 to subset 2 is observed starting from the lower boundary of the transition zone.

When the horizontal distance increases, the transition height is observed at higher distance between the EUT and the lap.

For the measured case 2 when the EUT is placed vertically on lap, the test results presented in section 3.7.2 show that, at each horizontal distance and for all measured heights:

- Subset 3 (grey line), with its beam directed away from the body, is operational almost all the time.

These test results confirm that the beam steering algorithm behaves in such a manner as to direct the energy away from the body while maintaining a good link budget.

4 Compliance Assessment

The goal of the tests presented in the previous sections is to determine the likelihood that energy would go towards or away from the human body during typical use.

It was demonstrated that in the vast majority of the cases, over typical usage/height/distances, the chosen subset directs energy away from the body.

As further supplemental compliance supporting information, numerical simulation results in Appendix A show that worst case power density is below the RF exposure FCC limit.

In Appendix A, we will present a worst case scenario defined using simulation, and supported by measurement in Appendix B. This case is "conservative" considering that the energy is always oriented toward the human body, which will be rarely observed in typical use as shown in Section 3.

Table 5 shows the simulated maximum spatially averaged power density, over 1cm^2 in the evaluation plane of the Intel 18265NGW module, embedded in the Dell model T02J.

Table 5 – Summary of simulation results for RF exposure compliance

Parameter	Value
Total conducted power	2 dBm
Maximum spatially averaged power density, over 1cm^2 - Simulation at 100% Duty Cycle	0.842 mW/cm^2
Maximum TX duty-cycle	70%
Maximum spatially averaged power density, over 1cm^2 - Simulation at 70% Duty Cycle	**0.589 mW/cm^2**

Therefore, with 0.589 mW/cm^2 spatially averaged power density value, Intel 18265NGW module, embedded in Dell model T02J, complies with FCC rule located in Title 47 of the Code of Federal Regulations (CFR) parts §2.1093 and §15.255(f).

The simulation results are supported by near field measurement using a near field probe. Because measurement results are unavailable at distances closer than 2 mm by probe limitation, the comparison between simulation and measurement is performed at 2 mm and 5 mm from the evaluation plane. The results are presented Appendix B.

Appendix A: Supplemental Numerical Modeling for RF Exposure Power Density Evaluation

A.1 Platform Simulation Methodology

A.1.1 Assessment considerations

During the system operation mode, it is challenging to define a practical system worst-case scenario in which the user is exposed to the highest emission level. To ensure coverage of the highest emission, the analysis of the worst-case corner condition is used and is emphasized in the following:

1. Platform orientation with respect to human body – In most of the cases, when the platform is very close to the human body, and the energy is directed to the human body, the human body will attenuate the signal. In this case, a reliable link can't be achieved. When a reliable link can't be maintained, the system enters search mode. In search mode, the system will transmit a low-duty cycle of less than 1%. This search mode contains signals which happen every 100ms at the maximum output power. However, in the analysis done for this document, the system is simulated in operational mode (not in search mode), operating at 70% duty cycle, which is much higher than the search mode.
2. Energy direction, beam forming – In order to avoid human body attenuation or object blockage of a reliable link, the system beam forming will automatically search for a path that will establish a more reliable link. So, in real life, in most of the cases the EM path will not be directed towards the human body (see Section 3). However, in the analysis presented in this document, worst-case beam forming direction is used.

Please note that the above worst-case assessment description is very conservative in that it is very unlikely that this case would happen under normal usage conditions. Since we cannot state with 100% certainty that this is impossible, we kept this worst-case assessment methodology for supplemental purposes. We ask that this be taken into consideration.

A.1.2 Near field and transition-zone field results

Finding the worst-case emission in the near field across the platform boundary requires searching on two orthogonal domains. One domain is the location – the need to find the place that has the worst-case energy. The other domain that has to be searched is the range of antenna phases – the need to search over the various antenna phases and find the antenna phase combination that gives the worst-case value. Section A.1.4 explains how these two worst-case (location and phase) searches are investigated.

After the completion of the worst-case phase analysis, the phases found during this analysis are used to find the worst-case spatially averaged power density across a $1cm^2$, for RF exposure evaluation purposes. EM simulation is used for this analysis.

Near-field analysis is simulated and correlated against measured lab results.

A.1.3 Simulation tool

A.1.3.1 Tool description

For the EM simulation, the commercially-available ANSYS Electronics Desktop 2016 (HFSS) is used. The ANSYS HFSS tool is used in the industry for simulating 3D, full-wave electromagnetic fields. Intel uses this EM simulation tool due to its gold-standard accuracy, advanced solver, and high-performance computing technology capabilities for doing accurate and rapid design of high-frequency components.

A.1.3.2 Solver description

The HFSS simulation is performed using the Finite Element Method, which operates in the frequency domain. The HFSS is based on an accurate direct solver with first order basis functions.

A.1.3.3 Convergence criteria and power density calculations

The HFSS uses a volume air box containing the simulated area to calculate the EM fields. The box is truncated by a Perfect Match Layer (PML) boundary condition. The simulation uses the adaptive mesh technique (see Figure 13) meet the exit criteria of delta S < 0.02. The delta S is the change in the magnitude of the S-parameters between two consecutive passes; if the magnitude and phase of all S-parameters change by an amount less than the Maximum-Delta-S-per-Pass value from one iteration to the next, the adaptive analysis stops.

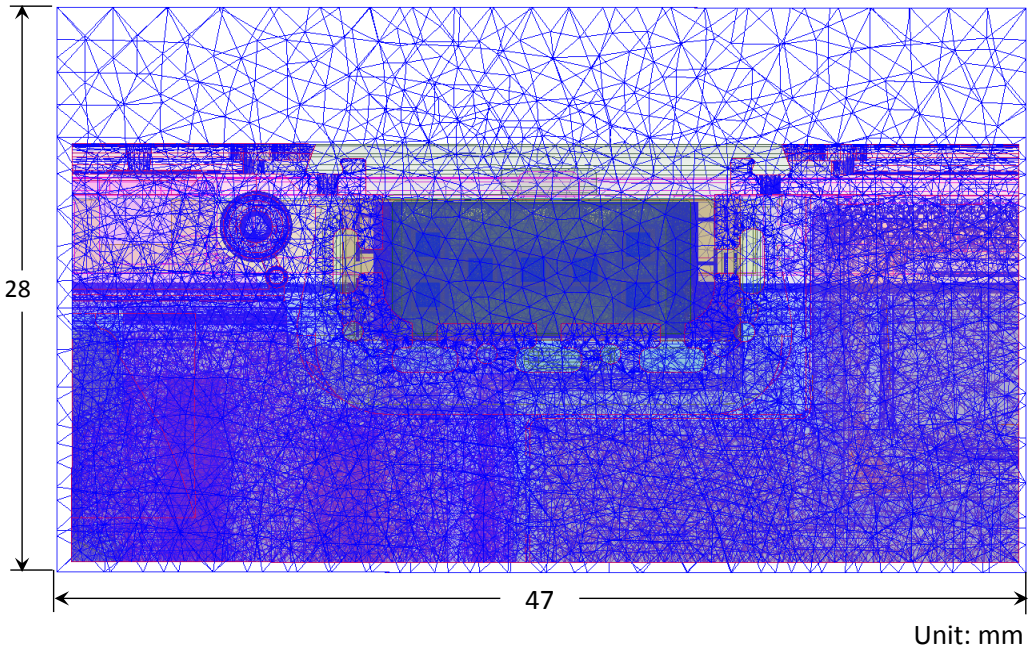

Figure 13 – Illustration of the adaptive mesh technique

After having the simulated electrical and magnetic (E and H) fields the Poynting vector is calculated in a grid with a 0.1 mm step. The spatially averaged power density on a given surface is calculated as the surface integral of the Poynting vector:

$$W = \frac{1}{2}\mathrm{Re}\int_S \left(\vec{E} \times \vec{H}^*\right) \cdot \vec{n} dS$$

Notes:

1. HFSS phasors in the field calculator are peak phasors, which leads to the ½ factor in the Poynting vector calculation.
2. Figure 13 is an illustration of the adaptive mesh technique and is presented in the context of simulation methodology presentation.

A.1.4 Finding the near-field, worst-case simulation configuration

As explained previously, near-field analysis requires finding the worst-case location (along the searched plane) and antenna phase values. As further explained, the search should be done on two domains:

1) Look for the worst-case position (across the search plane).
2) Look for the two worst-cases antenna phases.

Note: The search planes are defined as the planes used for the calculation of the two worst-cases antenna phase combinations. The new RFEM 3 antenna is intended to operate according to one of three predefined subsets[2]. For each subset an evaluation plane is defined taking into account the radiation direction of this subset. For subset 1 and 3 the evaluation plane corresponds to the tablet back–side exposure. For subset 2 the evaluation plane corresponds to the tablet front-edge exposure. The two domains described in 1) and 2) are applied for each subset separately in its evaluation plane in order to find worst case power density.

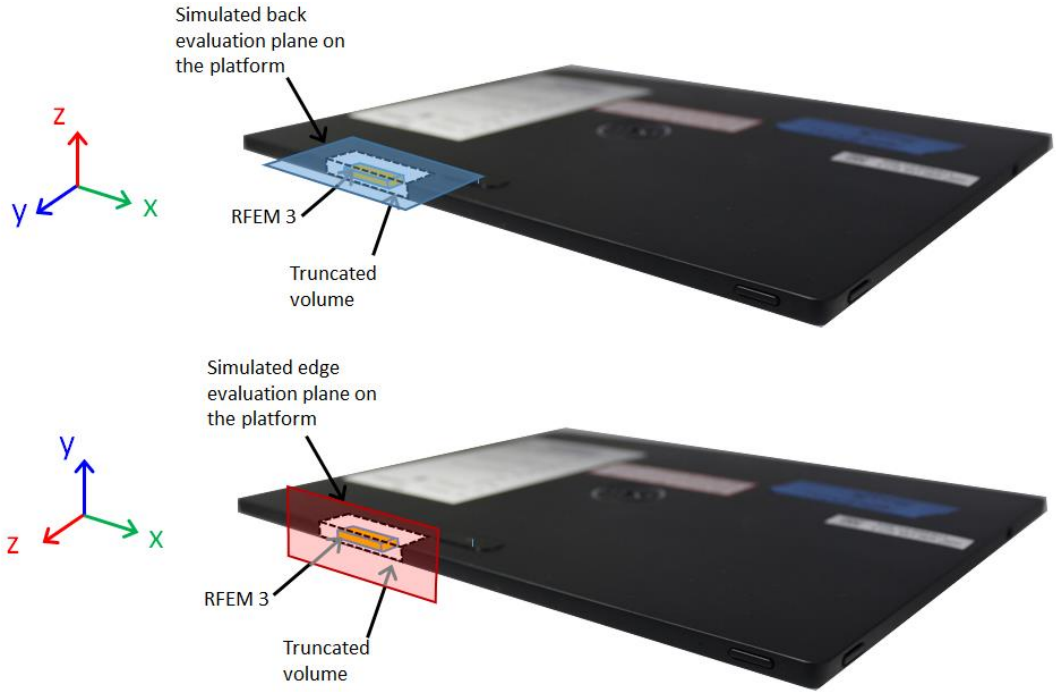

Figure 14 – The x-y search on the back evaluation plane (blue area) and edge evaluation plane (red area)

Note that for the xyz coordinate references used throughout this report, we always consider the z-axis as being towards the body direction. This consideration is used to conserve a general consistency for the field's representation and calculations in the worst-case determination procedure detailed below. In summary, the xy plane is the evaluation plane, and the z-axis is the vector in propagation direction towards the body.

[2] *A subset is a group of radiating elements which are excited simultaneously with the same amplitude. In RFEM 3, the number of subsets is three.*

A.1.4.1 Terminology

- Element – Each one of the radiating elements that are used in the system. We denote the antenna element with index **k** in this explanation.
- N – Number of chains (RFEM 3 includes 24 radiated antenna elements – **N**=24). As described in the previous section, there are three subsets in RFEM 3. These subsets, named subset 1, subset 2 and subset 3, are composed of 10, 11 and 11 active elements respectively. For each subset, a set of elements from the 24 radiating antennas is activated).
- Point – Each point on the grid that is used for searching for the worst- case position. They are spaced 0.1mm from each other. The grid point would be denoted as **g** in this explanation.
- Complex E field vector generated by the k[th] antenna element at point g:

$$\overrightarrow{E_{k,g}} = \vec{x}\left(\mathrm{Re}\left[E_{kx,g}\right] + j\mathrm{Im}\left[E_{kx,g}\right]\right) + \vec{y}\left(\mathrm{Re}\left[E_{ky,g}\right] + j\mathrm{Im}\left[E_{ky,g}\right]\right) + \vec{z}\left(\mathrm{Re}\left[E_{kz,g}\right] + j\mathrm{Im}\left[E_{kz,g}\right]\right)$$

- Complex H field vector generated by the k[th] antenna element at point g:

$$\overrightarrow{H_{k,g}} = \vec{x}\left(\mathrm{Re}\left[H_{kx,g}\right] + j\mathrm{Im}\left[H_{kx,g}\right]\right) + \vec{y}\left(\mathrm{Re}\left[H_{ky,g}\right] + j\mathrm{Im}\left[H_{ky,g}\right]\right) + \vec{z}\left(\mathrm{Re}\left[H_{kz,g}\right] + j\mathrm{Im}\left[H_{kz,g}\right]\right)$$

- $\hat{x}$, $\hat{y}$, $\hat{z}$ – unit direction vectors having unit magnitude and mutually orthogonal to each other.
- Without loss of generality in this explanation, RFEM 3 and the search plane are in the $\hat{x}$, $\hat{y}$ plane, and the integrated 1cm^2 plane is perpendicular to direction $\hat{z}$.

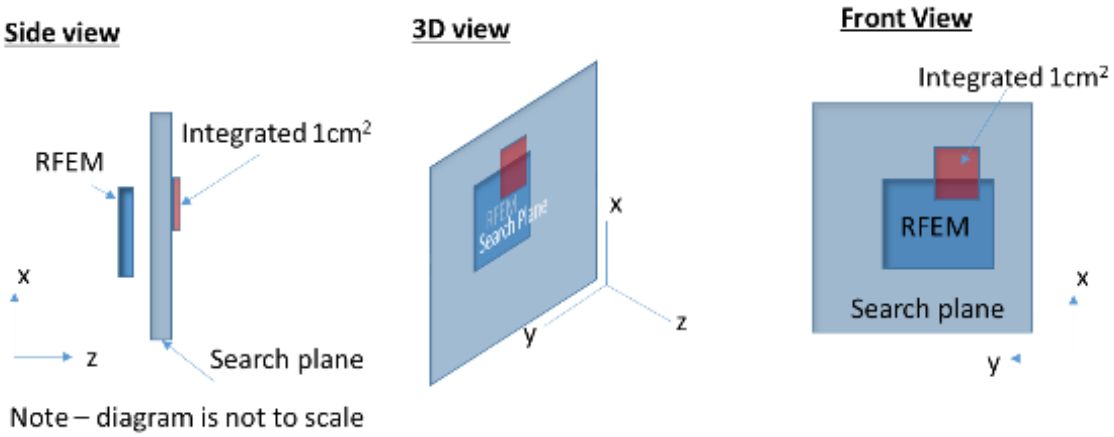

Figure 15 – Near field worst-case terminology and orientation

A.1.4.2 Primer on field vector representation

For each subset, *E* and *H* fields generated by the k chain are

$$\overrightarrow{E_k} = \vec{x}(\mathrm{Re}[E_{kx}] + j\mathrm{Im}[E_{kx}]) + \vec{y}\left(\mathrm{Re}\left[E_{ky}\right] + j\mathrm{Im}\left[E_{ky}\right]\right) + \vec{z}(\mathrm{Re}[E_{kz}] + j\mathrm{Im}[E_{kz}])$$

$$\overrightarrow{H_k} = \vec{x}(\mathrm{Re}[H_{kx}] + j\mathrm{Im}[H_{kx}]) + \vec{y}\left(\mathrm{Re}\left[H_{ky}\right] + j\mathrm{Im}\left[H_{ky}\right]\right) + \vec{z}(\mathrm{Re}[H_{kz}] + j\mathrm{Im}[H_{kz}])$$

For each subset, *E* and *H* fields generated by all *N* chains (only subset elements are activated) are

$$\overrightarrow{E_{\text{All}}} = \vec{x}\sum_{k=1}^{N}(\text{Re}[E_{kx}] + j\text{Im}[E_{kx}]) + \vec{y}\sum_{k=1}^{N}(\text{Re}[E_{ky}] + j\text{Im}[E_{ky}]) + \vec{z}\sum_{k=1}^{N}(\text{Re}[E_{kz}] + j\text{Im}[E_{kz}])$$

$$\overrightarrow{H_{\text{All}}} = \vec{x}\sum_{k=1}^{N}(\text{Re}[H_{kx}] + j\text{Im}[H_{kx}]) + \vec{y}\sum_{k=1}^{N}(\text{Re}[H_{ky}] + j\text{Im}[H_{ky}]) + \vec{z}\sum_{k=1}^{N}(\text{Re}[H_{kz}] + j\text{Im}[H_{kz}])$$

The Poynting vector generated by all *N* chains is

$$\begin{aligned}\overrightarrow{P_{\text{General,All}}} &= \frac{1}{2}\overrightarrow{E_{\text{All}}} \times \overrightarrow{H^{*}_{\text{All}}} \\ &= \frac{1}{2}\langle \vec{x}\left\{\sum_{k=1}^{N}(\text{Re}[E_{ky}] + j\text{Im}[E_{ky}])\sum_{k=1}^{N}(\text{Re}[H_{kz}] - j\text{Im}[H_{kz}])\right. \\ &\quad \left. - \sum_{k=1}^{N}(\text{Re}[E_{kz}] + j\text{Im}[E_{kz}])\sum_{k=1}^{N}(\text{Re}[H_{ky}] - j\text{Im}[H_{ky}])\right\} \\ &\quad + \vec{y}\left\{\sum_{k=1}^{N}(\text{Re}[E_{kz}] + j\text{Im}[E_{kz}])\sum_{k=1}^{N}(\text{Re}[H_{kx}] - j\text{Im}[H_{kx}])\right. \\ &\quad \left. - \sum_{i=1}^{N}(\text{Re}[E_{kx}] + j\text{Im}[E_{kx}])\sum_{k=1}^{N}(\text{Re}[H_{kz}] - j\text{Im}[H_{kz}])\right\} \\ &\quad + \vec{z}\left\{\sum_{k=1}^{N}(\text{Re}[E_{kx}] + j\text{Im}[E_{kx}])\sum_{k=1}^{N}(\text{Re}[H_{ky}] - j\text{Im}[H_{ky}])\right. \\ &\quad \left. - \sum_{k=1}^{N}(\text{Re}[E_{ky}] + j\text{Im}[E_{ky}])\sum_{k=1}^{N}(\text{Re}[H_{kx}] - j\text{Im}[H_{kx}])\right\}\rangle\end{aligned}$$

Power flow is

$$\begin{aligned}\text{Re}[\overrightarrow{P_{\text{General,All}}}] &= \frac{1}{2}\langle \vec{x}\left\{\sum_{k=1}^{N}\text{Re}[E_{ky}]\sum_{k=1}^{N}\text{Re}[H_{kz}] + \sum_{k=1}^{N}\text{Im}[E_{ky}]\sum_{k=1}^{N}\text{Im}[H_{kz}] - \sum_{k=1}^{N}\text{Re}[E_{kz}]\sum_{k=1}^{N}\text{Re}[H_{ky}]\right. \\ &\quad \left. - \sum_{k=1}^{N}\text{Im}[E_{kz}]\sum_{k=1}^{N}\text{Im}[H_{ky}]\right\} \\ &\quad + \vec{y}\left\{\sum_{k=1}^{N}\text{Re}[E_{kz}]\sum_{k=1}^{N}\text{Re}[H_{kx}] + \sum_{k=1}^{N}\text{Im}[E_{kz}]\sum_{k=1}^{N}\text{Im}[H_{kx}] - \sum_{k=1}^{N}\text{Re}[E_{kx}]\sum_{k=1}^{N}\text{Re}[H_{kz}]\right. \\ &\quad \left. - \sum_{k=1}^{N}\text{Im}[E_{kx}]\sum_{k=1}^{N}\text{Im}[H_{kz}]\right\} \\ &\quad + \vec{z}\left\{\sum_{k=1}^{N}\text{Re}[E_{kx}]\sum_{k=1}^{N}\text{Re}[H_{ky}] + \sum_{k=1}^{N}\text{Im}[E_{kx}]\sum_{k=1}^{N}\text{Im}[H_{ky}] - \sum_{k=1}^{N}\text{Re}[E_{ky}]\sum_{k=1}^{N}\text{Re}[H_{kx}]\right. \\ &\quad \left. - \sum_{k=1}^{N}\text{Im}[E_{ky}]\sum_{k=1}^{N}\text{Im}[H_{kx}]\right\}\rangle\end{aligned}$$

A.1.4.3 Domain search for worst-case direction

The two domain search is completed (for each subset) as follows:

A. First find a direction (location) for the worst-case 1cm^2 square averaging area using upper-bound methods.

   The basic concept behind the upper-bound method is to assume that there could be an "ideal beam forming" mechanism that could align the phases of all the elements for both E and H fields. (Obviously, in real life this cannot happen. This is the reason that this is an upper-bound method). When this ideal mechanism is used, then all the complex phasors are aligned to the same phase, hence the phasor absolute value can be used instead of the phasor. The E (and H) field for any direction is the sum of the magnitude of the fields (look at item 3, below, for a more formal description).

   This method provides the worst-case position independent of the antenna phases. It allows finding the worst-case location with this "ideal beam forming" mechanism.

   Item 3, below, translates the above verbal description into more formal mathematical wording.

B. After the worst-case direction is found using the upper-bound method for each subset, the antenna phases are aligned to this direction. The antenna phases are aligned to maximize the power across the 1cm^2 averaging area that was found using the upper-bound method. The method that is used to find the required antenna phases is as follows: first order the antennas of the subset according to the power contribution on the found 1cm^2 from the highest to the lowest. Then start by activating the antenna that contributes the most, set its phase to 0, and then activate the 2nd antenna and search over the phases for the 2nd antenna. Choose the phase that maximizes the power of the two antenna elements. To find the phase for the third antenna, fix antenna 1's phase to zero and antenna 2's phase to the value that was found before. Then search for the phases for the third antenna that maximize the power. Continue with the same process until you reach the last subset element. The same process is used to find the second worst case.

C. Calculate the power density with the antenna phases that were found in the previous item (item B).

The above process can be written as the following algorithm:

1. A grid is defined with 0.1mm spacing.
2. At each point in the grid, the complex E and H fields are calculated using each one of all radiating elements in the involved subset, separately. Each one of the calculated E and H fields are 3D complex vectors, so the simulation output from this stage is 10, 11, 11 3D complex E field strength vectors and 10, 11, 11 3D complex H field strength vectors for the three subsets respectively . The vectors are defined as:

$$\overrightarrow{E_{k,g}} = \vec{x}\left(\mathrm{Re}\left[E_{kx,g}\right] + j\mathrm{Im}\left[E_{kx,g}\right]\right) + \vec{y}\left(\mathrm{Re}\left[E_{ky,g}\right] + j\mathrm{Im}\left[E_{ky,g}\right]\right) + \vec{z}\left(\mathrm{Re}\left[E_{kz,g}\right] + j\mathrm{Im}\left[E_{kz,g}\right]\right) \text{ and}$$
$$\overrightarrow{H_{k,g}} = \vec{x}\left(\mathrm{Re}\left[H_{kx,g}\right] + j\mathrm{Im}\left[H_{kx,g}\right]\right) + \vec{y}\left(\mathrm{Re}\left[H_{ky,g}\right] + j\mathrm{Im}\left[H_{ky,g}\right]\right) + \vec{z}\left(\mathrm{Re}\left[H_{kz,g}\right] + j\mathrm{Im}\left[H_{kz,g}\right]\right)$$

3. Upper-bound assumption is used to derive the E and H field on each one of the grid points. The following items describe the upper-bound method that is used:
    a. The calculation is made separately for E field and H field.
    b. For E field, the following calculation is made independently for each one of the grid points:

$$\overrightarrow{E_{\mathrm{UB,g}}} = \vec{x}\sum_{k=1}^{N}\sqrt{\mathrm{Re}\left[E_{kx,g}\right]^2 + \mathrm{Im}\left[E_{kx,g}\right]^2} + \vec{y}\sum_{k=1}^{N}\sqrt{\mathrm{Re}\left[E_{ky,g}\right]^2 + \mathrm{Im}\left[E_{ky,g}\right]^2} + \vec{z}\sum_{k=1}^{N}\sqrt{\mathrm{Re}\left[E_{kz,g}\right]^2 + \mathrm{Im}\left[E_{kz,g}\right]^2} = \vec{x}\sum_{k=1}^{N}|E_{kx}| + \vec{y}\sum_{k=1}^{N}|E_{ky,g}| + \vec{z}\sum_{k=1}^{N}|E_{kz,g}|$$

    The magnitude of the complex E vector is summed over the antenna elements in a subset. The summation is done for each one of the grid points, and for each one of the elements in each direction, independently.
    c. The output of the previous item is the 3D real vector of the E field on each one of the simulated grid points in each direction. The physical implementation is that an ideal beam forming was done for the E field for each one of the points.
    d. The same process as described in item b is done for the H field.

$$\overrightarrow{H_{\mathrm{UB,g}}} = \vec{x}\sum_{k=1}^{N}\sqrt{\mathrm{Re}\left[H_{kx,g}\right]^2 + \mathrm{Im}\left[H_{kx,g}\right]^2} + \vec{y}\sum_{k=1}^{N}\sqrt{\mathrm{Re}\left[H_{ky,g}\right]^2 + \mathrm{Im}\left[H_{ky,g}\right]^2} + \vec{z}\sum_{k=1}^{N}\sqrt{\mathrm{Re}\left[H_{kz,g}\right]^2 + \mathrm{Im}\left[H_{kz,g}\right]^2} = \vec{x}\sum_{k=1}^{N}|H_{kx,g}| + \vec{y}\sum_{k=1}^{N}|H_{ky,g}| + \vec{z}\sum_{k=1}^{N}|H_{kz,g}|$$

    e. At each point in the grid, the Poynting vector is calculated by vector multiplication of the E and H fields, which are added up in items b and d. As explained before, without a loss of generality, we assume that the search plane is the x/y plane. All three (xyz) components of the Poynting vector are added, and not just the component that is normal to the x/y plane:

$$P_g = \frac{1}{2}Re\{(\vec{E}\times\vec{H}^*)\} = \frac{1}{2}Re\left\{\left(\left(E_yH_z^* - E_zH_y^*\right)\right)\hat{x} + \left((E_zH_x^* - E_xH_z^*)\right)\hat{y} + \left(E_xH_y^* - E_yH_x^*\right)\hat{z}\right)\right\}$$

$$P_{g,x} = \frac{1}{2}Re\{E_yH_z^* - E_zH_y^*\}$$

$$P_{g,y} = \frac{1}{2}Re\{(E_zH_x^* - E_xH_z^*)\}$$

$$P_{g,z} = \frac{1}{2}Re\{E_xH_y^* - E_yH_x^*\}$$

$$PUpperBound_g = \sqrt{{P_{g,x}}^2 + {P_{g,y}}^2 + {P_{g,z}}^2}$$

4. The above calculated Poynting vectors are used to estimate the power across 1cm^2 area.

$$P1cm2 = \iint_{1cm^2} PUpperBound_{g\ x,y,z}$$

5. The 1cm^2 area with the highest power value is used as the worst-case direction of a subset. The antenna phases are aligned to maximize the energy in this 1cm^2 area, as explained below in order to find the 2 worst cases:
    a. Turn on each element one-by-one to find order of power intensity in the 1cm^2 window. (Find the order of contribution)
    b. Sort in the power order from the highest to the lowest, #0 to #(10, 11, 11) for the involved subsets 1,2 and 3 respectively .
    c. Turn on #0 with phase P0=0. (reference)
    d. Turn on #1 and change the phase to maximize the power and find the phase P1.
    e. Keep P0 and P1 on, then turn on #2 and do same.
    f. Repeat for the rest of the antennas.
6. Using the antenna phases that were calculated in step 5, the power density is calculated along the evaluation plane and then spatially averaged across a 1cm^2 area.

A.1.5 3D models used in the simulation

A.1.5.1 Worst-case operating conditions of the platform

The Dell model T02J is a platform used in tablet mode. The worst case exposition to the radio frequency radiation can happen when the body of the user is in contact with the platform. Use cases such as lid-close, clam-shell, reading mode, video mode are not applicable for the worst exposure case assessment because the RFEM 3 antenna is placed on the top of the lid, therefore, only tablet mode is considered as the worst exposure case.

The two evaluation planes illustrated Figure 16 represents the evaluation planes according to subset radiation as mentioned in section A.1.4.

1. **Back-plane:** Is the evaluation plane for subset 1 and 3. In this case, the human body is below the base (blue area) – this mode represents the case in which a person holds the tablet and places it on their lap.
2. **Edge-plane:** Is the evaluation plane for subset 2. In this case, the human body is adjacent to platform edge (red area) – this mode represents the case in which a person is holding the tablet in their hand and the platform edge touching his body.

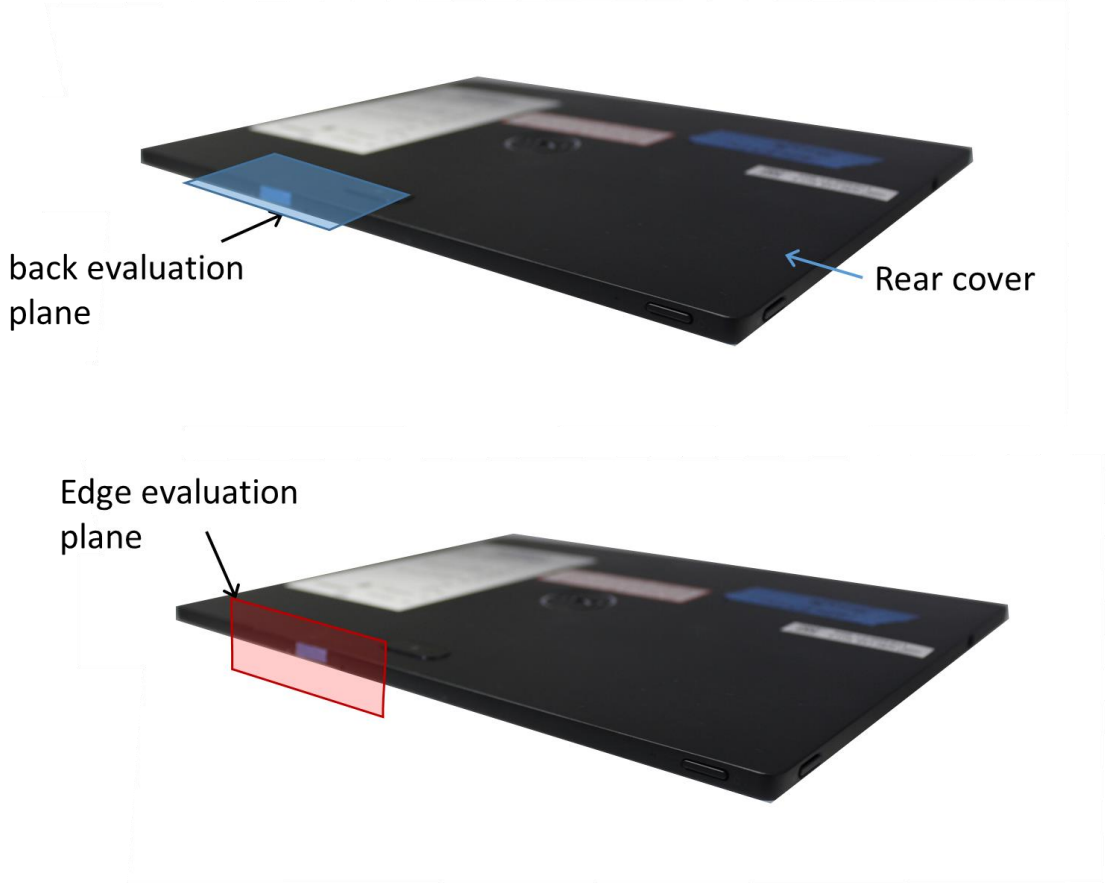

Figure 16 – Worst-case evaluation plane for Dell model T02J platform

A.1.5.2 RFEM 3 housing inside Intel 18265NGW module

The 3D Intel 18265NGW module is simulated inside the Dell T02J platform. Figure 17 shows the position of the RFEM 3 antenna, which is located inside the lid at the top left of the screen.

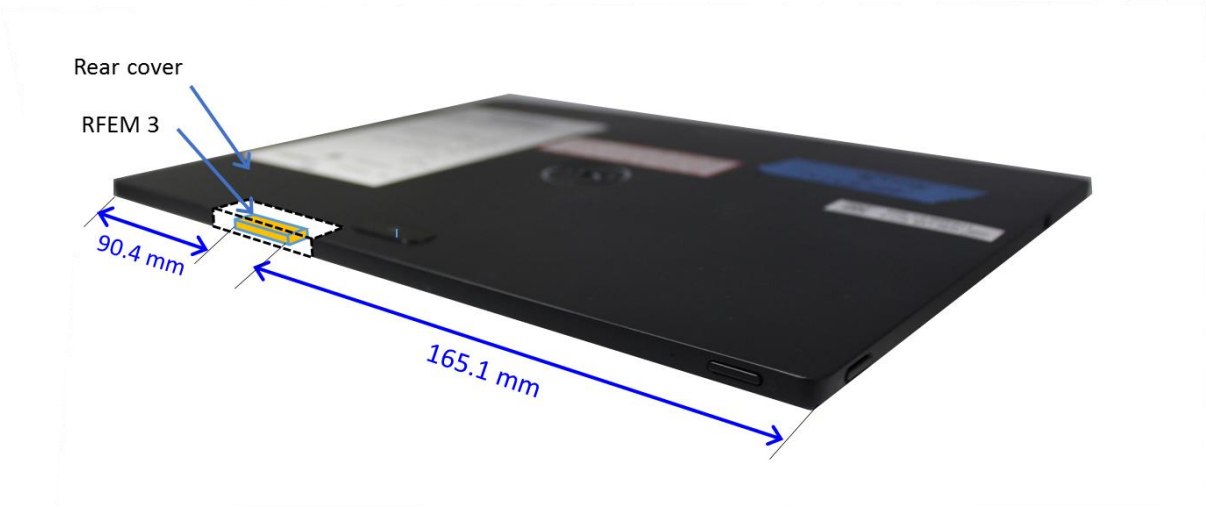

Figure 17 – Platform with RFEM 3 location

A.1.5.3 Closest distance to the body of an end user

In operating mode, the closest distance between the active antennas to the skin of an end user is when the person is holding the unit and touching the platform (at the evaluation plane) shown in Figure 16. In this case, two configuration were analyzed:

1. The human body is below the tablet – this mode represents the case in which a person places the tablet on their lap. In this scenario, the worst case emission is searched along the back evaluation plane (showed in blue in Figure 16) and the distance between human body to the active antenna is 2.25 mm.
2. The human body is adjacent to platform edge – this mode represents the case in which a person is holding the tablet in their hand and the tablet edge touching their body. In this scenario the worst case emission is searched along the edge plane (showed in red in Figure 16), in this case the distance between human body to the active antenna is 2.85 mm.

Figure 18 shows a cross-section (in the yz-plane) of the platform with the RFEM 3 inside the platform.

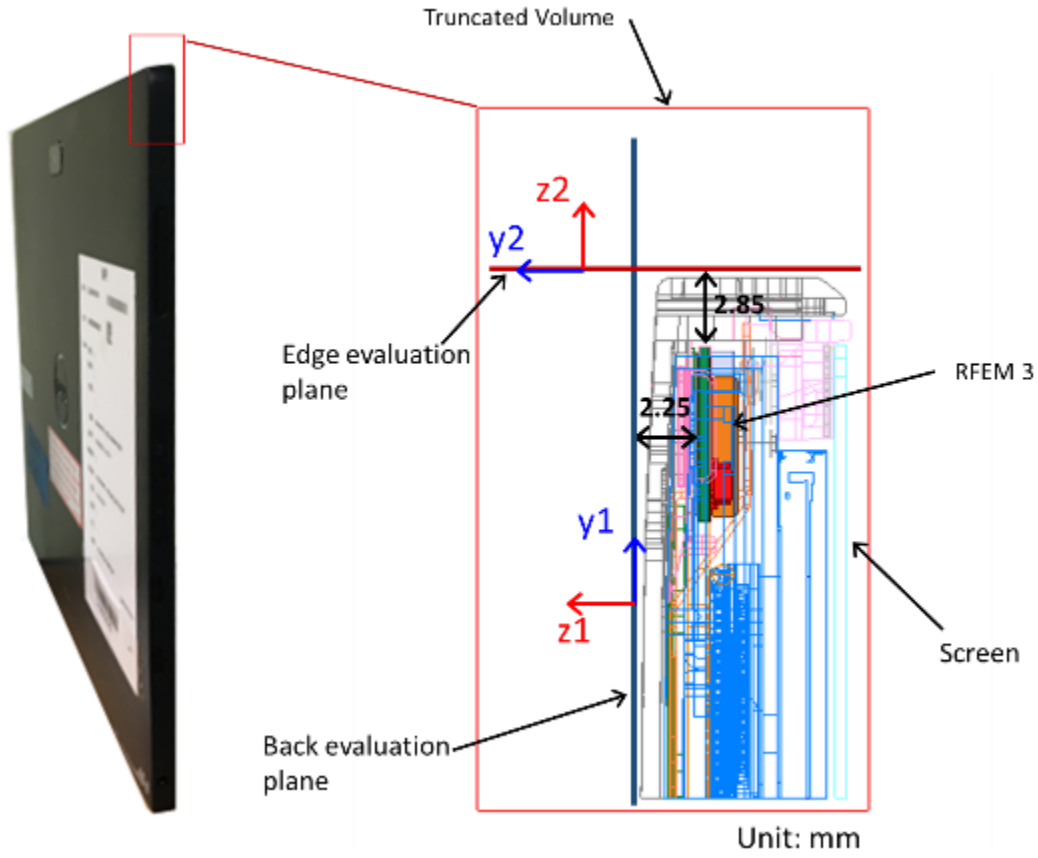

Figure 18 – Platform planes touching the body

A.1.5.4 Metals in proximity of the RFEM 3

All the metals that are in the RFEM 3 region (13.85 mm on each side) were included in the simulation.

A.1.6 Antenna feed

This section provides a general description of the numerical simulations; other details of the simulation geometry are included in reference [1]. The EM simulation uses an accurate 3D model of the RFEM 3 antenna. The model includes the antenna elements as well as their feeding lines.

In the simulation (as well as in the product), each antenna element is fed independently, and we excite the antennas at the origin of the antenna structure on the RFEM 3. (The antenna structure includes the silicon chip, the solder bumps, the vias, traces and actual antenna element.)

As described previously, the RFEM 3 antenna will be operated according to one of three predefined subsets. For the operational subset, signals of equal amplitude are applied to the feed-points of individual array elements, and the aggregate equivalent conducted power to all array elements *c*orresponds to the sum of all elements' powers. In the worst-case power density the subset 1 is the operational subset with an equivalent conducted power of 2 dBm; thus each element is fed by -8 dBm (2 dBm divided over ten elements).

The total power (same per element) is used to build the pattern of radiated power through beam forming. For building the beam forming pattern, the same power is used per element, while phase is changed per element. (Refer to Section 2.2 for more information about beam forming). Phases are derived for each excitation separately, to simulate the worst-case condition. Section A.1.4 explains how the phases are derived to find the worst case condition.

A.2 Power Density Simulation Results

A.2.1 Introduction

The evaluation planes presented in Section A.1.5.2 has been simulated according to the methodology described in Section A.1. The simulation results for all subsets in the concerned evaluation planes are presented in this section.

The power density has been simulated over three channels with frequencies listed in Table 6. For each channel, we'll present the resulting details according to the methodology explained in Section A.1.4:

- Simulation results of the upper bound single-point power density for each single-point across the mesh ($PUpperBound_g$). Please note that this value represents single-point power density and not spatially averaged power density over 1cm^2. Even though a 1mW/cm^2 scale is used, this value represents an upper-bound power density for each single point of the mesh, which is a much smaller area than 1cm^2.
- The results of the single-point power density using the antenna phases corresponding to the first and second worst-cases.
- Spatially averaged power density over 1cm^2 results of the first and second worst-case for each subset antenna phases. These results present the spatially averaged power density across 1cm^2 using the xyz components of the Poynting vector.
- All results for all channels and subsets are normalized to the taget maximum power of 2dBm

Table 6 – WiGig channel frequencies

	Channel 1	Channel 2	Channel 3
Frequency (GHz)	58.32	60.48	62.64

Table 7 summarizes all the simulation configurations as well as the result types presented in this section:

Table 7 – Power density simulation configuration and result details

Subset	Evaluation Plane	Channels	Results types	Count	Reference
Subset 1	Back-plane	1, 2, and 3	Upper-bound power density	3 channels x 3 Subsets	Table 8
			1st worst-case antenna phases	3 channels x 3 Subsets	Table 9
Subset 2	Edge-plane		2nd worst-case antenna phases	3 channels x 3 Subsets	Table 10
			single point power density	2 Worst cases x 3 channels x 3 Subsets	Table 11
Subset 3	Back-plane		spatially averaged power density	2 Worst cases x 3 channels x 3 Subsets	Table 12
			Worst-case distribution(1)	[3 plots] – Very worst case	Section A.2.6

(1) The distribution of the found worst case spatially averaged power density among the 18 calculated worst cases.

A.2.2 Upper bound power density values in the evaluation plane

The Upper Bound single-point power density is calculated for each subset of the antenna. Table 8 summarizes, for all subsets, the maximum calculated upper bound single point power density.

Please note that since the worst-case conditions are searched over a plane for near field, then the azimuth and the elevation are not relevant. The worst-case position is calculated using all the power density single-points issued from the upper-bound simulation results. We leverage the phase conditions for each antenna element that resulted in these worst-case conditions to evaluate final spatially averaged power density. The mathematical basis for using these as the worst-case phase conditions to evaluate the final spatially averaged power density is provided in Section A.1.4.3.

Table 8 – Maximum upper bound single point power density [mW/cm²]

	Channel 1	Channel 2	Channel 3
Subset 1	30.793	31.668	26.350
Subset 2	17.643	22.909	22.453
Subset 3	21.308	19.929	16.078

A.2.3 Worst-case antenna phases in the evaluation plane

The phase's configurations a.k.a. 'beamforming codes' for the first and second worst power density cases are calculated for each subset and each channel using the phase search algorithm detailed in bullet 5 of Section A.1.4.3.

Table 9 and Table 10 shows, for each channel, the phases of each subset elements (marked in grey) in the first and second worst power density case respectively. The white cells with phase ("-") correspond to the non-active elements of the subset. For instance, for subset 1, the active elements are 7, 8; 17 to 24 and the worst case occurs for each channel with the indicated phases. "Ph #" indicates the number of the attributed phase combination for each worst case.

Note: The final antenna phases worst cases, used later in measurement, corresponds to the four highest maximum spatially averaged power density values among the eighteen calculated worst cases (3 channels x 3 subsets x 2 first worst-cases) showed in Table 12.

Table 9 –Phases configurations for the first worst case for all antenna subsets

Antenna index	Subset 1 – Back plane Phases [Degrees]			Subset 2 – Edge plane Phases [Degrees]			Subset 3 – Back plane Phases [Degrees]		
	CH1	CH2	CH3	CH1	CH2	CH3	CH1	CH2	CH3
	Ph #1	Ph #2	Ph #3	Ph #4	Ph #5	Ph #6	Ph #7	Ph #8	Ph #9
1	-	-	-	-	-	-	90	0	180
2	-	-	-	-	-	-	0	180	0
3	-	-	-	-	-	-	0	180	0
4	-	-	-	270	270	0	-	-	-
5	-	-	-	0	0	0	-	-	-
6	-	-	-	270	180	270	-	-	-
7	90	90	90	-	-	-	-	-	-
8	0	270	90	-	-	-	-	-	-
9	-	-	-	180	270	90	-	-	-
10	-	-	-	90	180	90	-	-	-
11	-	-	-	180	270	90	-	-	-
12	-	-	-	0	180	270	-	-	-
13	-	-	-	90	270	180	180	90	270
14	-	-	-	270	90	0	90	0	270
15	-	-	-	180	90	180	90	0	180
16	-	-	-	0	180	270	180	270	180
17	90	180	180	-	-	-	-	-	-
18	180	180	180	-	-	-	-	-	-
19	180	180	180	-	-	-	-	-	-
20	0	0	0	-	-	-	-	-	-
21	270	0	270	-	-	-	270	90	270
22	0	90	0	-	-	-	0	180	0
23	0	180	0	-	-	-	0	270	90
24	180	0	180	-	-	-	180	90	270

Table 10 –Phases configurations for the second worst case for all antenna subsets

Antenna index	Subset 1 – Back plane Phases [Degrees]			Subset 2 – Edge plane Phases [Degrees]			Subset 3 – Back plane Phases [Degrees]		
	CH1	CH2	CH3	CH1	CH2	CH3	CH1	CH2	CH3
	Ph #10	Ph #11	Ph #12	Ph #13	Ph #14	Ph #15	Ph #16	Ph #17	Ph #18
1	-	-	-	-	-	-	180	0	270
2	-	-	-	-	-	-	0	180	90
3	-	-	-	-	-	-	0	0	0
4	-	-	-	270	270	270	-	-	-
5	-	-	-	0	0	0	-	-	-
6	-	-	-	180	270	0	-	-	-
7	0	90	90	-	-	-	-	-	-
8	270	270	90	-	-	-	-	-	-
9	-	-	-	180	0	180	-	-	-
10	-	-	-	90	180	270	-	-	-
11	-	-	-	180	270	180	-	-	-
12	-	-	-	0	270	0	-	-	-
13	-	-	-	180	180	0	270	90	0
14	-	-	-	0	180	0	90	0	0
15	-	-	-	270	90	270	90	0	0
16	-	-	-	90	180	270	0	270	270
17	270	180	270		-	-	-	-	-
18	270	180	180		-	-	-	-	-
19	0	180	180	-	-	-	-	-	-
20	270	0	0	-	-	-	-	-	-
21	270	0	0	-	-	-	270	90	0
22	0	90	90	-	-	-	0	180	90
23	270	180	90	-	-	-	0	270	180
24	90	180	270	-	-	-	180	90	0

A.2.4 Single-Point power density values in the evaluation plane

Table 11 presents, for all channels and subsets, the calculated single-point power density values in the concerned evaluation plane using the first and the second worst-case subset antenna phases presented in Table 9 and Table 10 respectively (18 Worst cases).

Table 11 – Maximum single point power density [mW/cm^2]

	First worst case			Second worst case		
	Channel 1	**Channel 2**	**Channel 3**	**Channel 1**	**Channel 2**	**Channel 3**
Subset 1	3.987	3.296	2.825	3.643	2.551	2.964
Subset 2	1.269	2.021	1.037	1.201	1.412	1.425
Subset 3	2.805	2.335	2.403	2.164	2.651	2.485

A.2.5 Spatially averaged power density over 1 cm^2 values in the evaluation plane

Table 12 shows, for all channels and subsets, the calculated spatially averaged power density over 1 cm^2 at 100% duty cycle (Eigteen Calculated worst cases). These values are calculated in the concerned evaluation plane using the first and the second worst-case subset antenna phases shown in Table 9 and Table 10 respectively. The 6 highest spatially averaged power density are marked in bold in Table 11. Simulated field and power density distributions at the evaluation plane are provided for the six configurations in Section A.2.7.

Table 12 – Maximum spatially averaged power density over 1cm^2 [mW/cm^2]

	First worst case			Second worst case		
	Channel 1	**Channel 2**	**Channel 3**	**Channel 1**	**Channel 2**	**Channel 3**
Subset 1	**0.842**	0.744	0.630	**0.840**	0.739	0.628
Subset 2	**0.427**	0.385	0.340	0.305	**0.355**	0.300
Subset 3	**0.612**	0.534	0.450	**0.592**	0.486	0.419

Table 12 shows that the very worst case is found for **subset 1 at channel 1**(marked in orange) with spatially averaged power density of **0.842 mW/cm^2** at 100 % duty cycle. The next section presents all power density distributions for this worst cases.

A.2.6 Worst case power density distribution

As described in the previous section, the worst case spatially averaged power density over 1 cm^2 among the eighteen calculated worst-cases is found for subset 1, channel 1. The worst case subset antenna phase's configuration used in this case is for the first worst case (see Table 9, subset 1 / channel 1 configuration).

This section present for this worst case the distribution of the following listed items:

- Upper bound single point power density distribution
- Single-point power density distribution
- One dimensional cut of the single-point power density distribution
- Spatially averaged power density over 1 cm^2

A.2.6.1 Upper-bound power density distribution

Figure 19 presents upper-bound, single-point power density of subset 1, channel 1 which is the worst case among the two simulated worst cases of the three subsets. The evaluation plane of subset 1 is the back-plane represented in Figure 12.

The footprint of the platform components in the back evaluation plane for single-point power density representation is shown in Figure 21.

Worst-case coordinates on channel 1 are X=0.030 cm, Y=-0.040 cm.

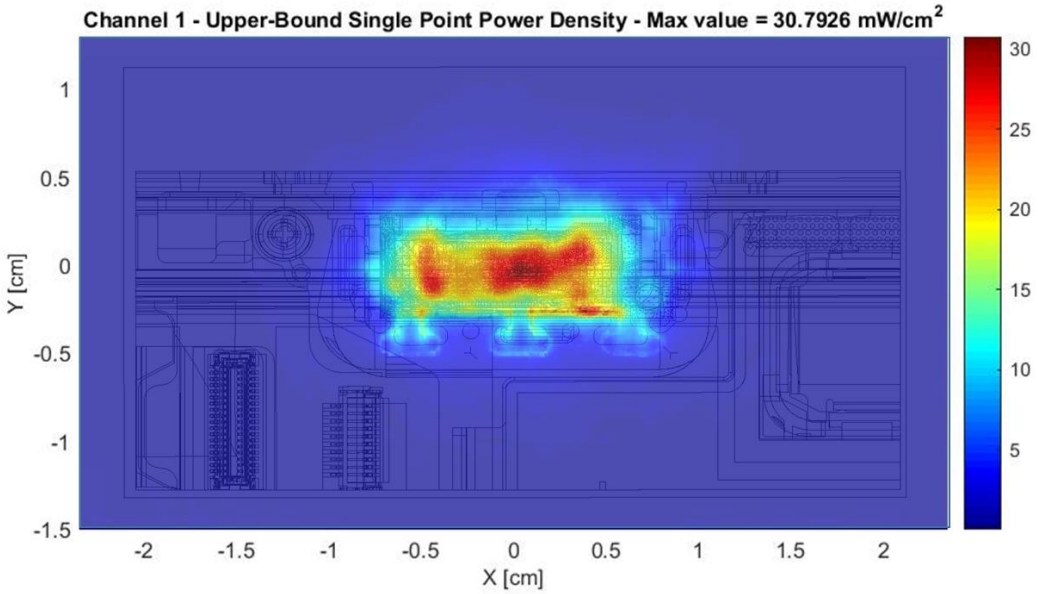

Figure 19 – Channel 1 upper-bound, single-point power density- subset 1

A.2.6.2 Single point power density distribution

Figure 20 presents the single-point power density distribution of subset 1, channel 1 in the back-plane using the worst-case antenna phases of subset 1 (see Table 9)

The footprint of the platform components in the back plane for single-point power density representation is shown in Figure 21.

Worst-case coordinates on channel 1 are X=0.270, cm Y=0.020 cm.

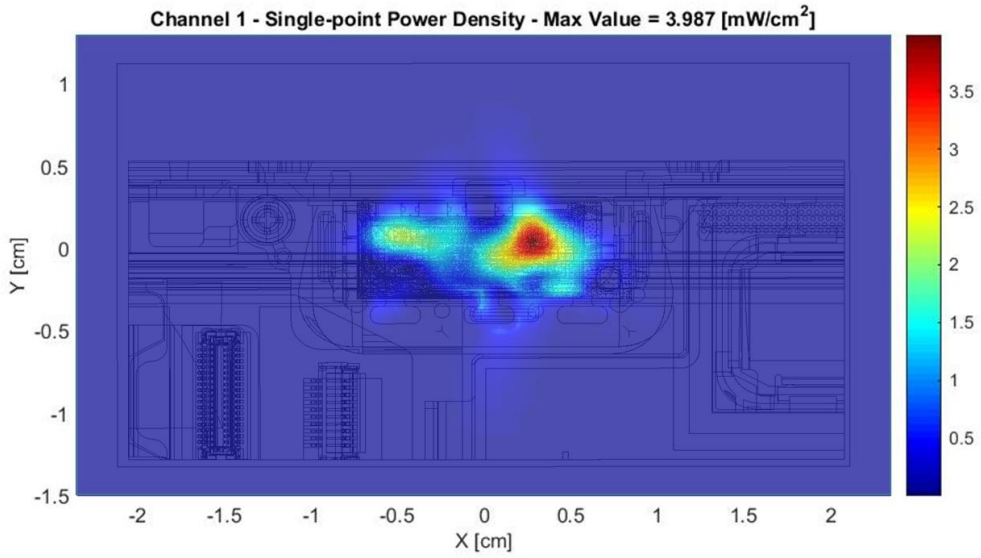

Figure 20 – Channel 1 single-point power density - subset 1

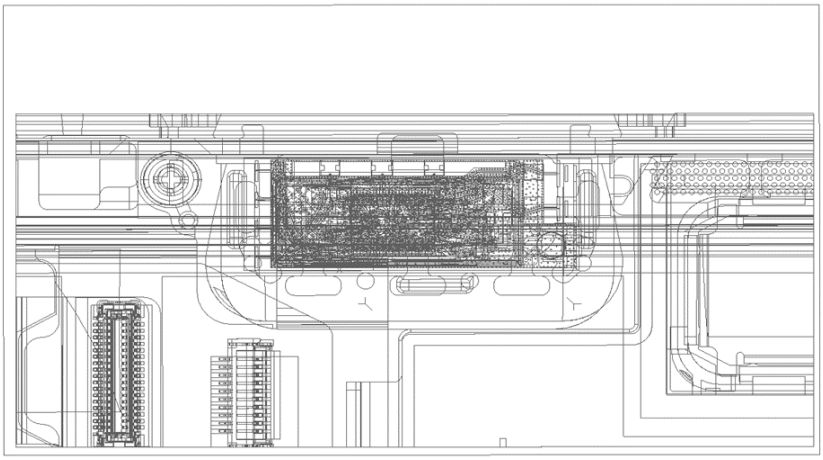

Figure 21 – Footprint of single-point power density plane representation

A.2.6.3 One dimensional cut of the single-point power density distribution

In Figure 22 and Figure 23, we present the simulation results from the xyz components of single-point power density values with worst-case antenna phases of subset 1, channel 1 which is the worst case among the three subsets. The figures represent a 1-dimensional cut in the x-axis and y-axis that shows the behavior of the near field power density at the evaluation plane.

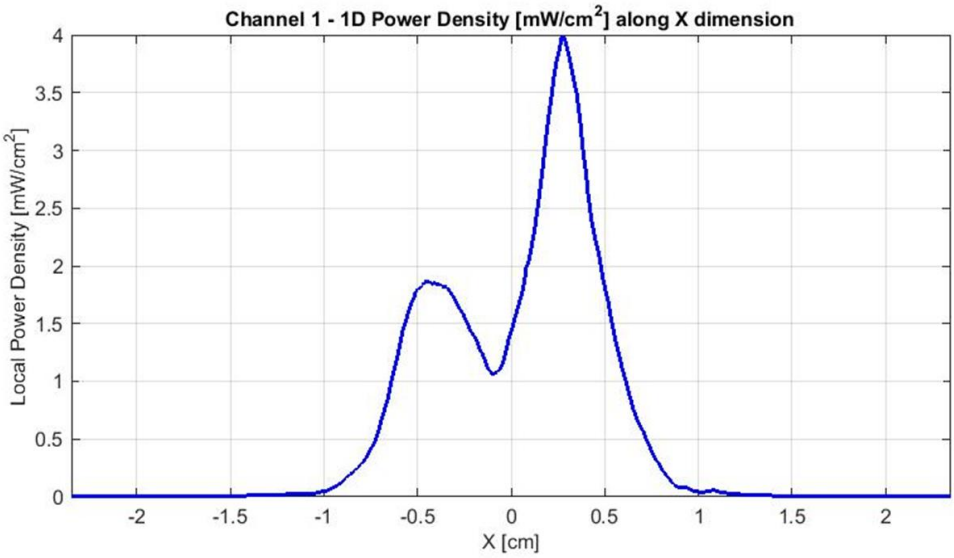

Figure 22 – 1-dimensional plots of the power density along x dimension

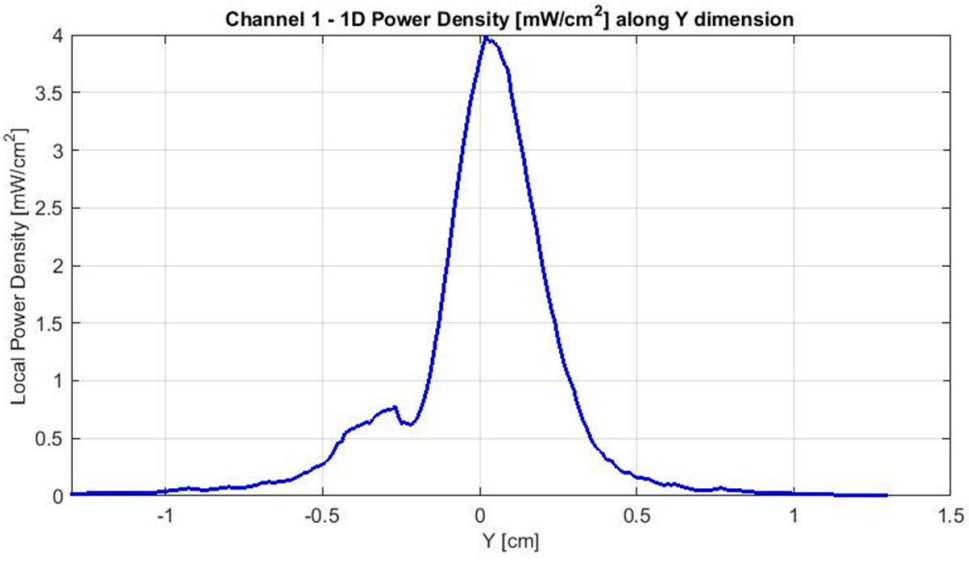

Figure 23 – 1-dimensional plots of the power density along y dimension

A.2.6.4 Distribution of Spatially averaged power density over 1 cm²

Figure 24 presents the spatially averaged power over 1cm² at 100% duty cycle for the worst-case scenario of subset 1, channel 1 as explained in Section A.1.4.3.

The 1cm² square location correspondent to the maximum of spatially averaged power density value is plotted in Figure 24 for the channel 1.

Worst-case coordinates on channel 1 are X=0.040, cm Y=-0.030 cm.

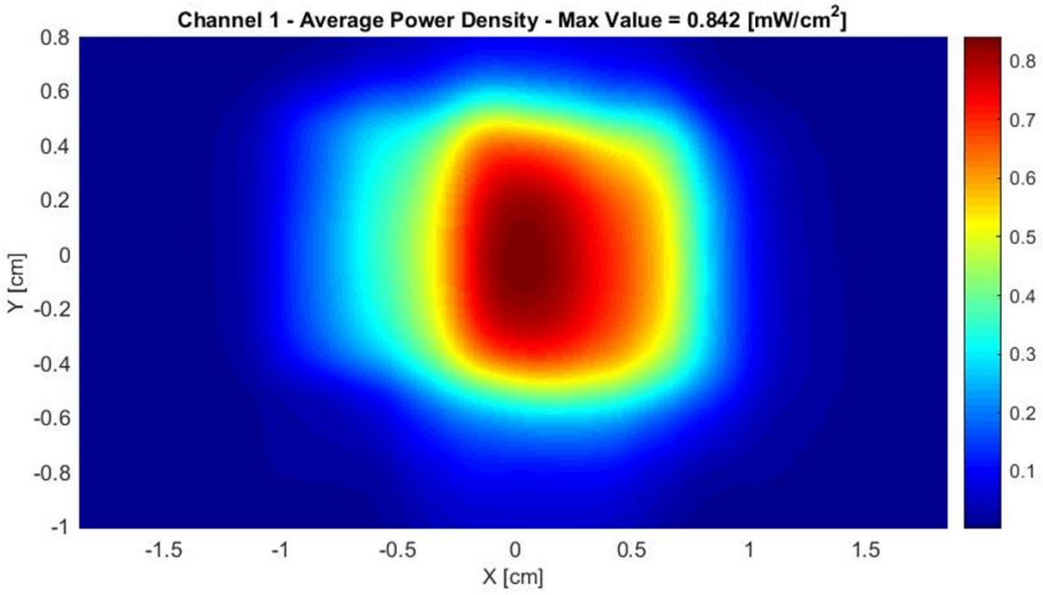

Figure 24 – Channel 1– spatially averaged power density over 1cm2 - subset 1

The Table 13 shows the simulated worst-case power density, for subset 1 – channel 1, in the evaluation plane.

Table 13 – Worst-case power density – Subset 1

Highest power density	Subset 1 - Channel 1
70% duty cycle	0.589
100% duty cycle	0.842

Notes for Table 13

1. The worst-case power density is found for channel 1 on subset 1.
2. The Maximum power density (spatially averaged over worst 1cm²) in channel 1 is achieved at 0 mm distance from the platform boundary and equals 0.842 mW/cm² over 100% duty cycle.
3. As explained in Section 2.4, the Intel 18265NGW module is limited to transmit at a duty cycle of 70% over 10 seconds. Therefore the maximum spatially-integrated and time-averaged power density over 1cm² is 0.842 x 0.7 = 0.589 mW/cm².

A.2.7 Field and Power Density Distributions for the Six Highest Worst Cases

This section shows the E-field, H-field, local power density and spatially averaged power density distribution at the corresponding evaluation plane of the six highest worst cases spatially averaged power density determined in section A.3.5 and marked in bold in Table 11.

The table below list the identified highest six- spatially averaged power density worst cases

Table 14 – Highest six worst-case spatially averaged power density

	Subset	Channel	Worst-case	Simulated AVG. PD	Phase config	Plot
Worst-Case #1	1	1	1	0.842	Ph #1	Plot #1
Worst-Case #2	1	1	2	0.840	Ph #10	Plot #2
Worst-Case #3	2	1	1	0.427	Ph #4	Plot #3
Worst-Case #4	2	2	2	0.355	Ph #14	Plot #4
Worst-Case #5	3	1	1	0.612	Ph #7	Plot #5
Worst-Case #6	3	1	2	0.592	Ph #16	Plot #6

Plot # 1: First worst case - Subset 1 – Channel 1

Evaluation Plane: Back-plane

Frequency: 58320 MHz

Distance: 0mm

Simulated E-field
Maximum value = 176.837 V/m - Peak

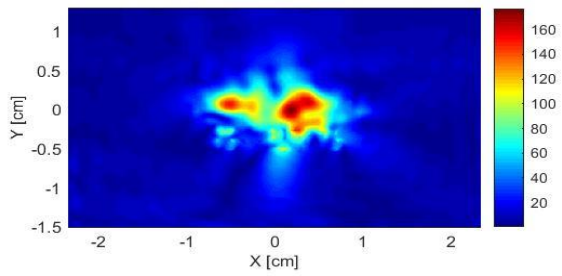

Simulated H-field
Maximum value = 0.544 A/m - Peak

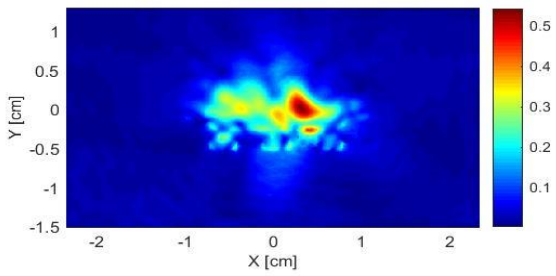

Simulated localized free space power density
Maximum value = 3.987 mW/cm^2

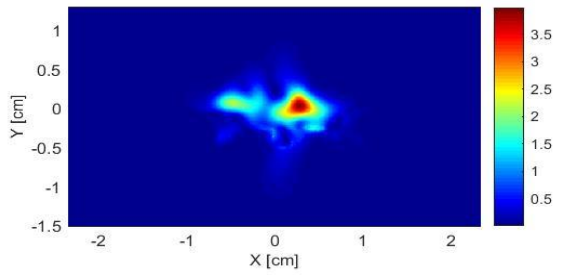

Simulated spatially Averaged power density
Maximum value = 0.842 mW/cm^2

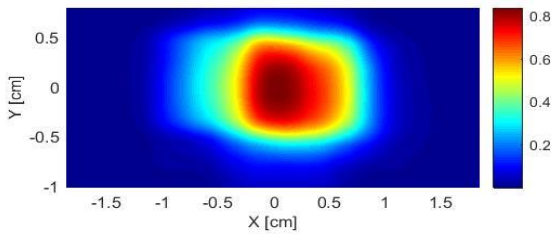

Plot # 2: Second worst case - Subset 1 – Channel 1

Evaluation Plane: Back plane

Frequency: 58320 MHz

Distance: 0mm

Simulated E-field
Maximum value = 169.538 V/m - Peak

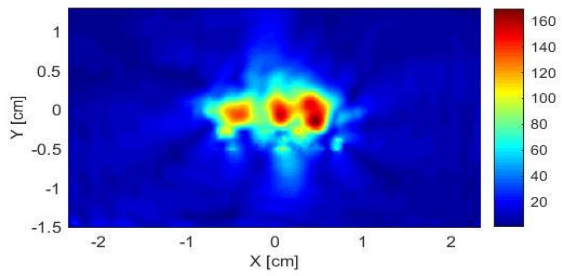

Simulated H-field
Maximum value = 0.502 A/m - Peak

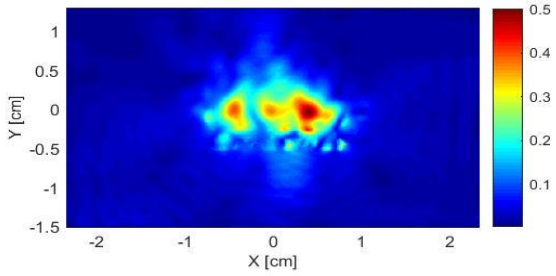

Simulated localized free space power density
Maximum value = 3.643 mW/cm^2

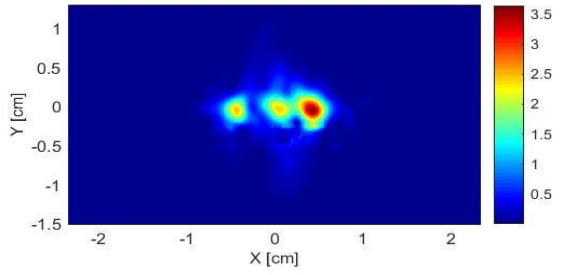

Simulated spatially Averaged power density
Maximum value = 0.840 mW/cm^2

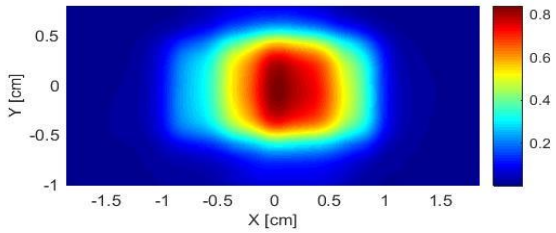

Plot # 3: First worst case - Subset 2 – Channel 1

Evaluation Plane: Edge plane

Frequency: 58320 MHz

Distance: 0mm

Simulated E-field
Maximum value = 164.356 V/m - Peak

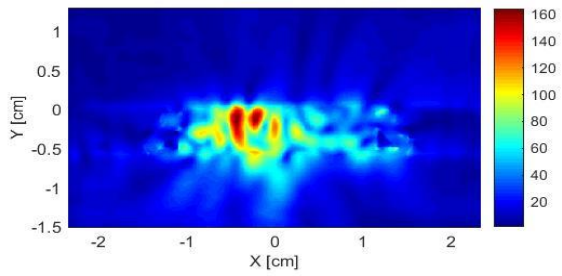

Simulated H-field
Maximum value = 0.442 A/m - Peak

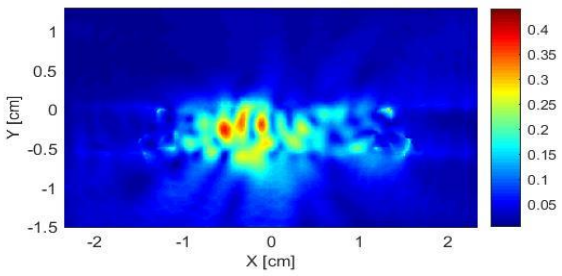

Simulated localized free space power density
Maximum value = 1.269 mW/cm^2

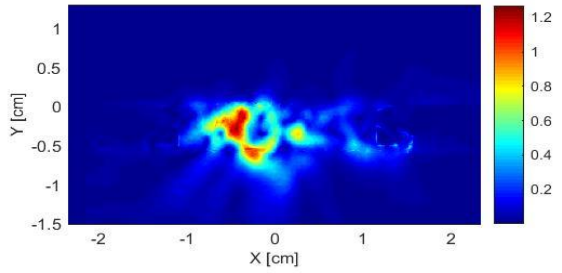

Simulated spatially Averaged power density
Maximum value = 0.427 mW/cm^2

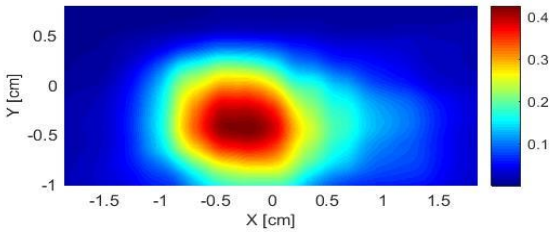

Plot # 4: Second worst case - Subset 2 – Channel 2

Evaluation Plane: Edge plane

Frequency: 60480 MHz

Distance: 0mm

Simulated E-field
Maximum value = 135.111 V/m - Peak

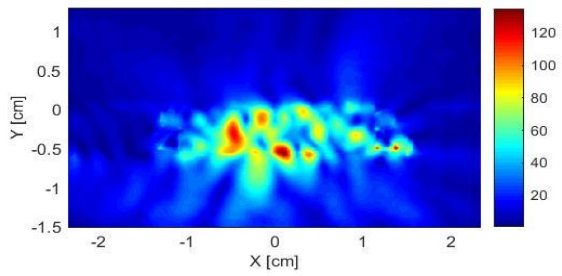

Simulated H-field
Maximum value = 0.312 A/m - Peak

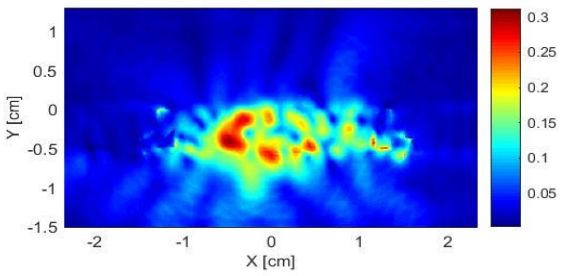

Simulated localized free space power density
Maximum value = 1.412 mW/cm^2

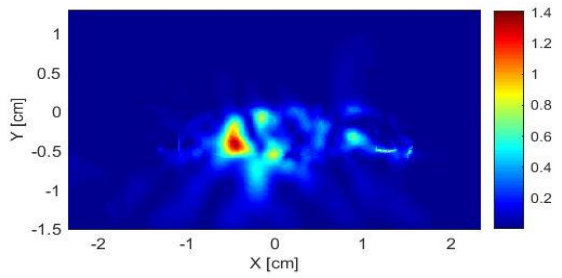

Simulated spatially Averaged power density
Maximum value = 0.355 mW/cm^2

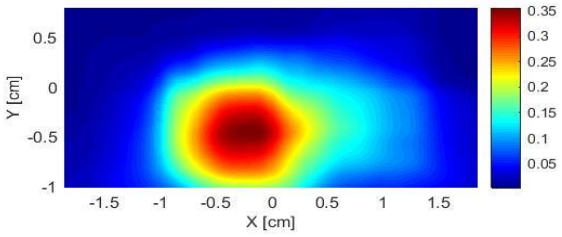

Plot # 5: First worst case - Subset 3 – Channel 1

Evaluation Plane: Back plane

Frequency: 58320 MHz

Distance: 0mm

Simulated E-field
Maximum value = 158.208 V/m - Peak

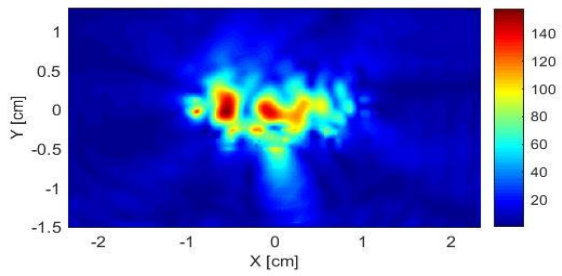

Simulated H-field
Maximum value = 0.461 A/m - Peak

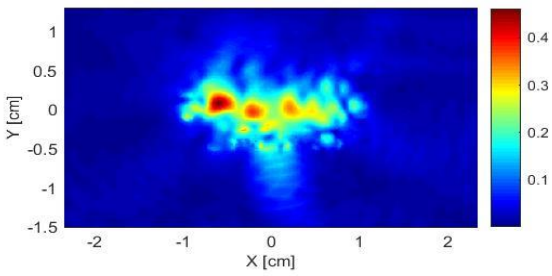

Simulated localized free space power density
Maximum value = 2.805 mW/cm^2

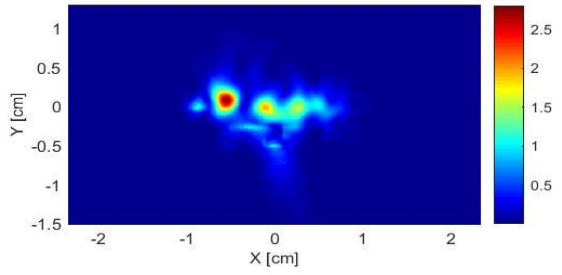

Simulated spatially Averaged power density
Maximum value = 0.612 mW/cm^2

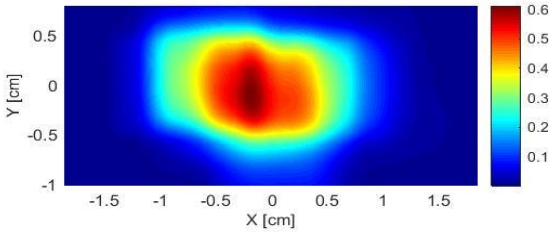

Plot # 6: Second worst case - Subset 3 – Channel 1

Evaluation Plane: Back plane

Frequency: 58320 MHz

Distance: 0mm

Simulated E-field
Maximum value = 143.204 V/m - Peak

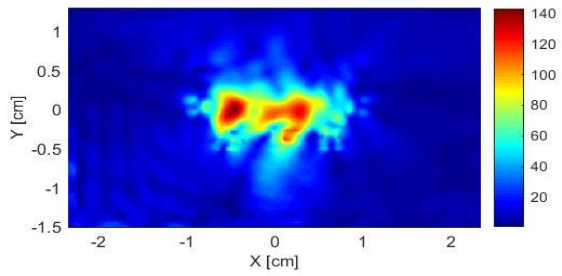

Simulated H-field
Maximum value = 0.384 A/m - Peak

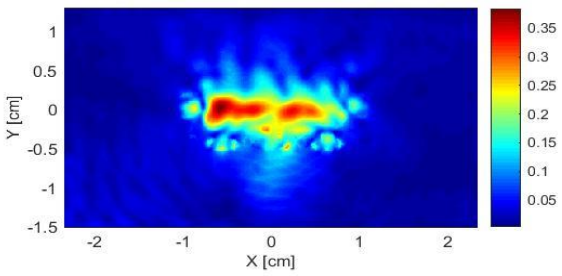

Simulated localized free space power density
Maximum value = 2.164 mW/cm^2

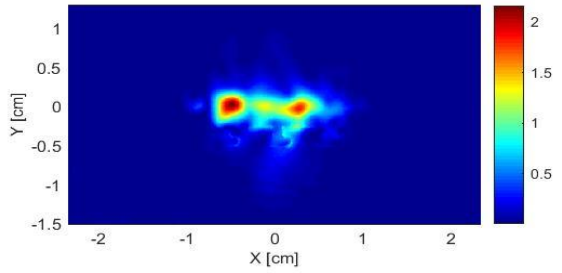

Simulated spatially Averaged power density
Maximum value = 0.592 mW/cm^2

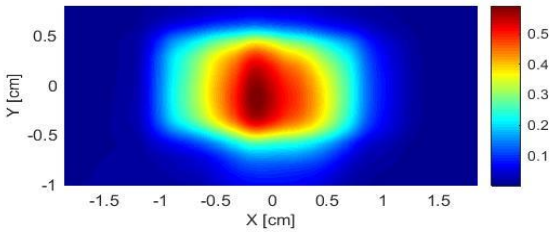

A.2.8 Simultaneous Transmission Evaluation for SAR and Power Density

The first step in determining whether the composite-system end product qualifies for exclusion from simultaneous transmit RF exposure measurement, the sum of the ratios of the exposure levels to their limits is considered. In this case, the WiGig antennas operating in the 60 GHz frequency band are co-located with two WLAN antennas according to FCC ID PD918265NGU, test report number SAR20170207 dated Feb, 8-11, 2017.

Considering the Max SAR of the WLAN module is 1.29 W/Kg and the max power density for the WiGig module is 0.589mW/cm^2, the sum of the ratios is:

$$(1.29 / 1.6) + (0.589 / 1) = 1.395 > 1$$

Because the sum of the ratios is greater than 1, figure 21 shows that the SAR and Power density peak locations and distribution contours are sufficiently separated, implying the applicability of the evaluation by selecting the highest exposure ratio in terms of spatial peak SAR or spatially averaged/spatial peak power density in accordance with the applicable exposure limits. Thus:

$$(1.29 / 1.6) \textbf{ OR } (0.589 / 1) = 0.806 < 1$$

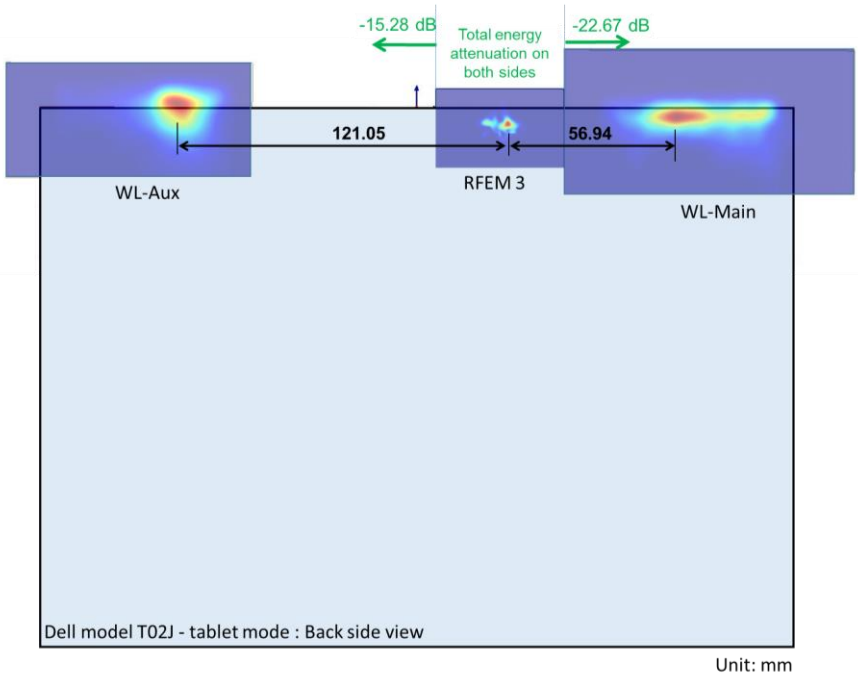

Figure 25 – SAR and Power Density Distribution for co-located antennas

A.2.9 Conclusion

The simulation results for the three subsets in the concerned evaluation plane for three channels were presented in this report. The worst case is observed on channel 1 for subset 1, with the maximum total spatially averaged power density of 0.589 mW/cm^2. Note that the applicable FCC limit is 1 mW/cm^2.

Appendix B: Near-Field Measurements supporting the RF Exposure Power Density simulations

B.1 Introduction

In this section, the near field power density measurement performed using the worst case antenna phases found by simulation is presented. This near field measurement supports the simulation presented in Section A.2. Indeed, because the measurement results are unavailable at distances closer than 2 mm, the comparison between simulation and measurement is performed at 2 mm and 5 mm from the evaluation plane.

A near-field RF exposure system from SPEAG is used to perform these measurements.

B.2 Probe Characteristics

The probe consist of two dipoles (0.8 mm length) optimally arranged with different angles (γ1 and γ2) to obtain pseudo-vector information, printed on glass substrate protected by high density foam that allows low perturbation of the measured field.

Three or more measurements are taken for different probe rotational angles, deriving the amplitude and polarization information.

The probe's characteristics are illustrated in Table 15

Table 15 – Near Field probe Characteristics

Frequency Range	[3]
Length	320 mm
Probe tip external diameter	8 mm
Probe's two dipoles length	0.9mm – Diode loaded
Probe's substrate	Quartz 0.9 x 20 x 0.18mm (εr=3.8)
Distance between diode sensors and probe's tip	1.5 mm
Axial Isotropy	±0.6 dB
Maximum operating E-field	3000 V/m
Lower E-field detection threshold	5 V/m @ 60 GHz
Minimum Mechanical separation between probe tip and a Surface	0.5mm
Calibration reference point	Diode Sensor

More details about the measurement system are found in reference [2].

[3] *The probe calibration range is 750 MHz – 90 GHz*

B.3 Total Field and Power Flux Density Reconstruction

Computation of the power density in general requires knowledge of the electric (E-) and magnetic (H-) field amplitudes and phases in the plane of incidence. Reconstruction of these quantities from pseudo-vector E-field measurements is feasible, as they are constrained by Maxwell's equations.

The reconstruction algorithm developed by the system manufacturer, together with the ability of the probe to measure extremely close to the source without perturbing the field, permits reconstruction of the E- and H-fields as well as of the power density on measurement planes located as near as 0.5mm away in the frequency band of 60 GHz.

The average of the reconstructed power density is evaluated over a circular area in each measurement plane. The area of the circle is defined by the user; the default is 1 cm^2.

B.4 Measurement configurations

The near field measurement is performed on the four highest maximum spatially averaged power density found among the eighteen calculated worst cases (3 channels x 3 subsets x 2 first worst-cases) showed in Table 12. The test configurations are summarized in Table 16.

Table 16 – Test Configuration

<table>
<tr><th colspan="2">Measurement Configuration</th></tr>
<tr><td>EUT</td><td>Dell Model T02J</td></tr>
<tr><td>Measured cases</td><td>Four highest worst cases* found in simulation:
<table>
<tr><th></th><th>Subset</th><th>Channel</th><th>Worst-case</th><th>Distance [mm]</th><th>Phase Config.*</th></tr>
<tr><td>Case 1#</td><td>1</td><td>1</td><td>1</td><td>2, 5</td><td>Ph #1</td></tr>
<tr><td>Case 2#</td><td>1</td><td>1</td><td>2</td><td>2, 5</td><td>Ph #10</td></tr>
<tr><td>Case 3#</td><td>3</td><td>1</td><td>1</td><td>2, 5</td><td>Ph #7</td></tr>
<tr><td>Case 4#</td><td>3</td><td>1</td><td>2</td><td>2, 5</td><td>Ph #16</td></tr>
</table></td></tr>
<tr><td>Measurement Distances / Resolution</td><td>2 mm / 1.29 mm
5 mm / 1.29 mm</td></tr>
<tr><td>Scan Plane</td><td>4.23 x 4.23 cm^2</td></tr>
</table>

* See Table 9 and Table 10.

B.5 Measurement results

Tables 15 through 18 show the comparison between simulation and measurement for the four measured worst-cases at 2 and 5 mm distances from the evaluation plane. Simulation and measurement are both peak phasors. All results are calculated at 100 % duty cycle. Simulation is using square averaging and measurement is using circular averaging.

Table 17 – Case 1#: Simulation Vs. test results @ 2 and 5 mm.

	Measurement Distance (mm)	Simulated	Measured	Max. Deviation (dB)
E-field (V/m)	2 mm	116.795	131.203	1.010
	5 mm	85.640	92.877	0.705
H-field (A/m)	2 mm	0.313	0.348	0.934
	5 mm	0.267	0.362	2.651
Single-point PD (mW/cm^2)	2 mm	1.946	1.856	0.204
	5 mm	1.038	1.388	1.262
Average PD (mW/cm^2)	2 mm	0.593	0.445	1.247
	5 mm	0.435	0.353	0.908

Table 18 – Case 2#: Simulation Vs. test results @ 2 and 5 mm.

	Measurement Distance (mm)	Simulated	Measured	Max. Deviation (dB)
E-field (V/m)	2 mm	123.700	120.954	0.195
	5 mm	95.050	113.322	1.527
H-field (A/m)	2 mm	0.331	0.315	0.411
	5 mm	0.274	0.342	1.931
Single-point PD (mW/cm^2)	2 mm	2.108	1.884	0.488
	5 mm	1.391	1.444	0.162
Average PD (mW/cm^2)	2 mm	0.562	0.417	1.296
	5 mm	0.392	0.386	0.072

Table 19 – Case 3#: Simulation Vs. test results @ 2 and 5 mm.

	Measurement Distance (mm)	Simulated	Measured	Max. Deviation (dB)
E-field (V/m)	2 mm	97.048	136.279	2.949
	5 mm	78.574	87.247	0.909
H-field (A/m)	2 mm	0.271	0.280	0.308
	5 mm	0.186	0.242	2.323
Single-point PD (mW/cm^2)	2 mm	1.259	1.904	1.794
	5 mm	0.848	0.836	0.060
Average PD (mW/cm^2)	2 mm	0.457	0.379	0.812
	5 mm	0.349	0.231	1.796

Table 20 – Case 4#: Simulation Vs. test results @ 2 and 5 mm.

	Measurement Distance (mm)	Simulated	Measured	Max. Deviation (dB)
E-field (V/m)	2 mm	100.302	102.463	0.185
	5 mm	73.658	76.436	0.322
H-field (A/m)	2 mm	0.241	0.265	0.814
	5 mm	0.194	0.182	0.585
Single-point PD (mW/cm^2)	2 mm	1.158	0.871	1.233
	5 mm	0.780	0.682	0.584
Average PD (mW/cm^2)	2 mm	0.392	0.198	2.970
	5 mm	0.299	0.166	2.548

Figures below show the comparison at 2 mm and 5 mm from the evaluation plane, between the simulation and the near field measurement in terms of E-Field, H-Field, Single-point Power Density and Spatially Averaged Power Density at 100 % duty cycle for the four higher worst cases.

Note that the fields results presented in the figures below consider a peak phasor for electromagnetic fields **for both simulation and measurement.**

Case #1 - DISTANCE = 2 mm	
Simulated	**Measured**
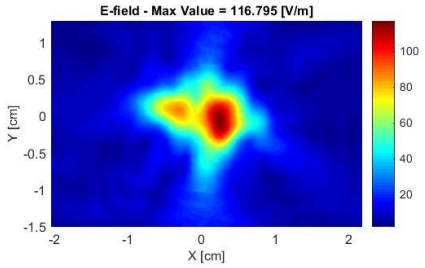	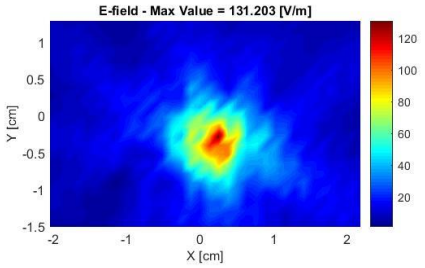
E-field (V/m) @ 2 mm – Deviation of Max Value: 1.010 dB	
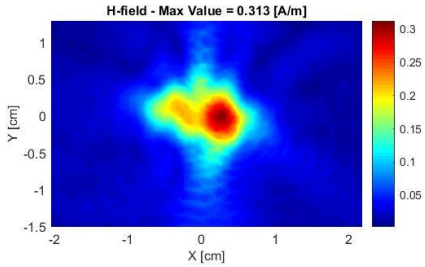	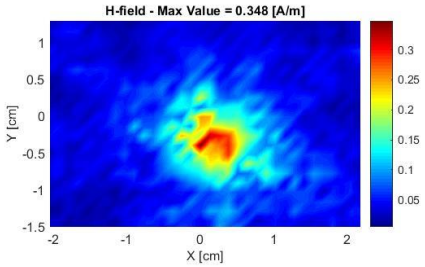
H-field (V/m) @ 2 mm – Deviation of Max Value: 0.934 dB	
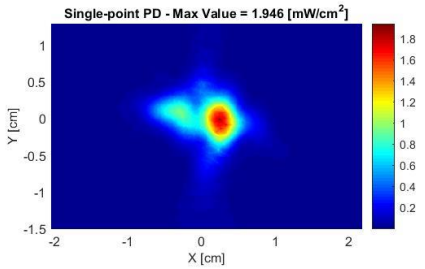	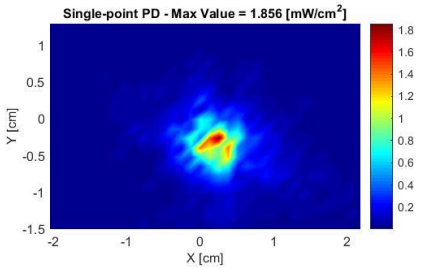
Localized free space PD (mW/cm2) @ 2 mm – Deviation of Max Value: 0.204 dB	
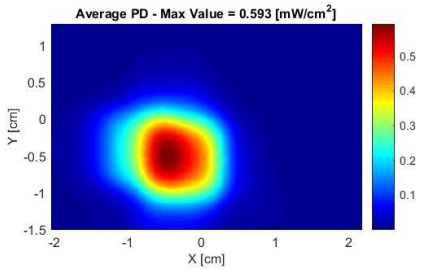	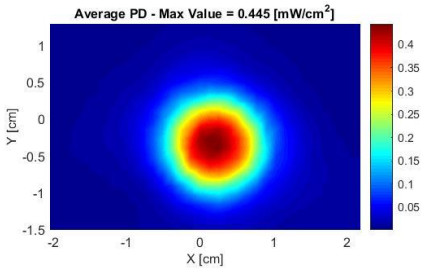
Spatially Averaged PD (mW/cm2) @ 2 mm – Deviation of Max Value: 1.247 dB	

Case #1 - DISTANCE = 5 mm	
Simulated	**Measured**
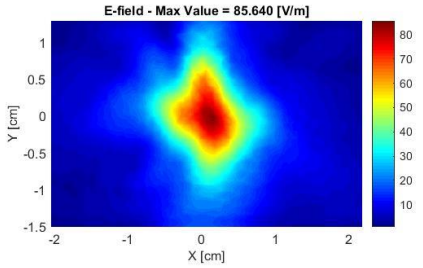	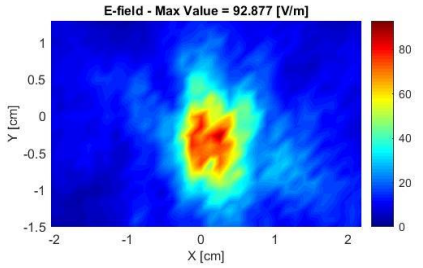
E-field (V/m) @ 5 mm – Deviation of Max Value: 0.705 dB	
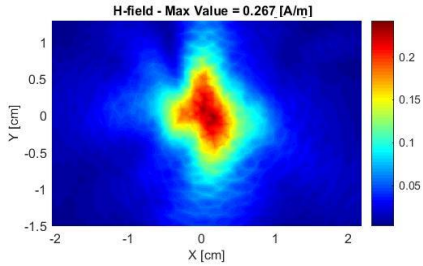	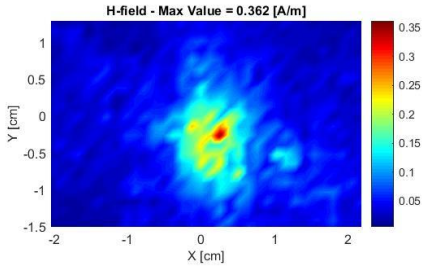
H-field (V/m) @ 5 mm – Deviation of Max Value: 2.651 dB	
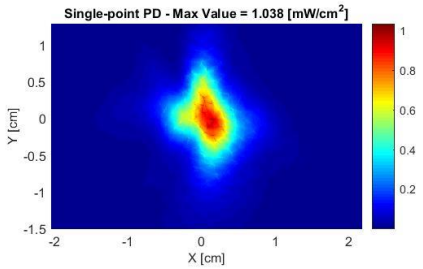	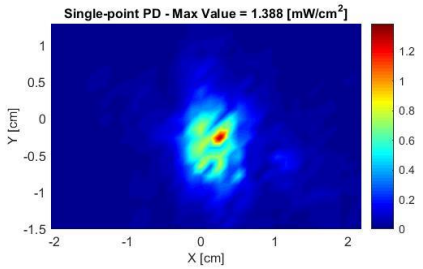
Localized free space PD (mW/cm2) @ 5 mm – Deviation of Max Value: 1.262 dB	
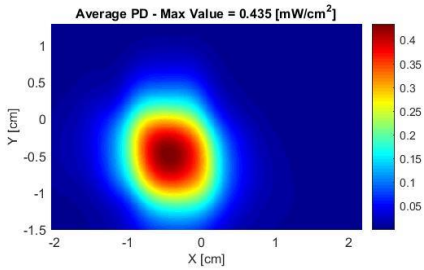	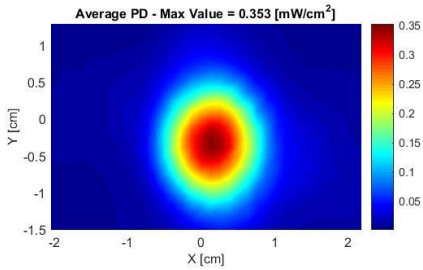
Spatially Averaged PD (mW/cm2) @ 5 mm – Deviation of Max Value: 0.908 dB	

Case #2 - DISTANCE = 2 mm	
Simulated	**Measured**
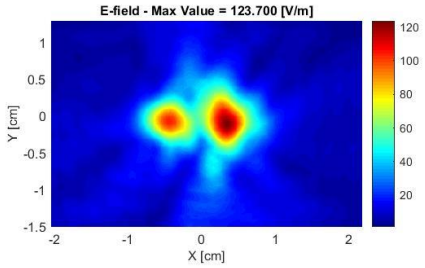	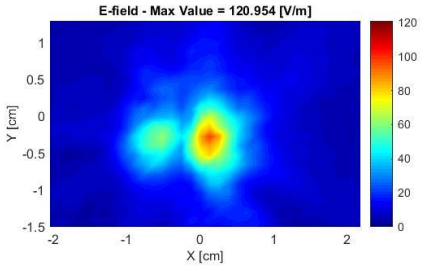
E-field (V/m) @ 2 mm – Deviation of Max Value: 0.195 dB	
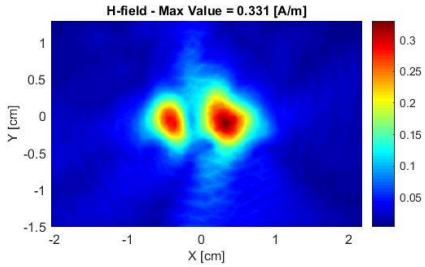	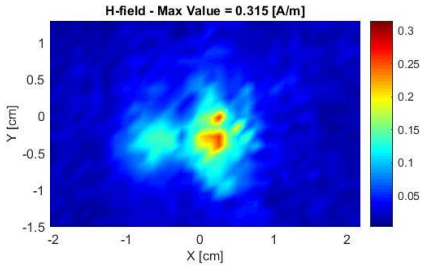
H-field (V/m) @ 2 mm – Deviation of Max Value: 0.411 dB	
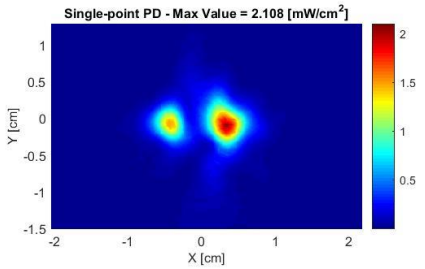	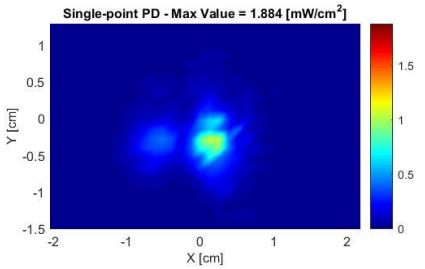
Localized free space PD (mW/cm2) @ 2 mm – Deviation of Max Value: 0.488 dB	
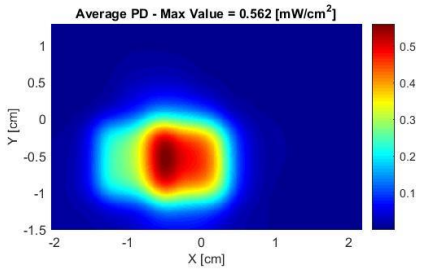	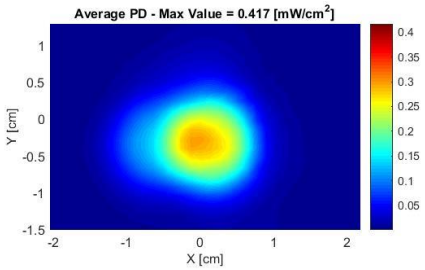
Spatially Averaged PD (mW/cm2) @ 2 mm – Deviation of Max Value: 1.296 dB	

Case #2 - DISTANCE = 5 mm	
Simulated	**Measured**
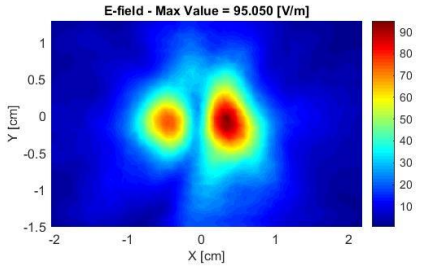	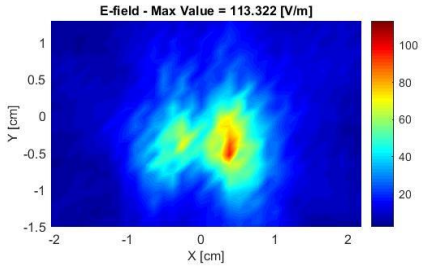
E-field (V/m) @ 5 mm – Deviation of Max Value: 1.527 dB	
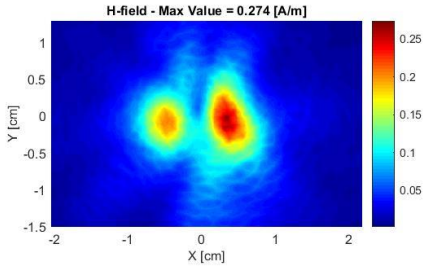	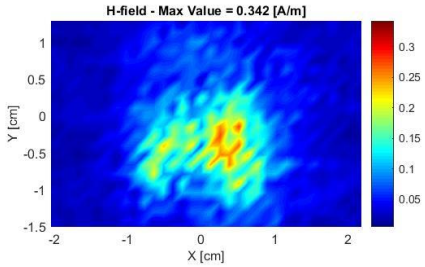
H-field (V/m) @ 5 mm – Deviation of Max Value: 1.931 dB	
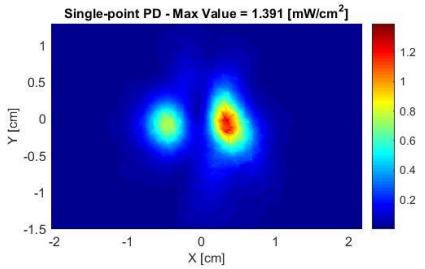	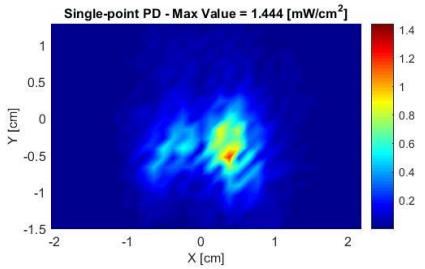
Localized free space PD (mW/cm2) @ 5 mm – Deviation of Max Value: 0.162 dB	
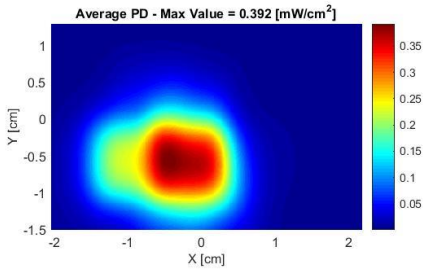	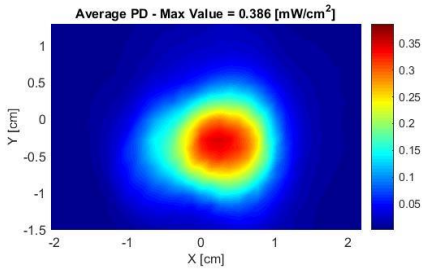
Spatially Averaged PD (mW/cm2) @ 5 mm – Deviation of Max Value: 0.072 dB	

Case #3 - DISTANCE = 2 mm	
Simulated	**Measured**
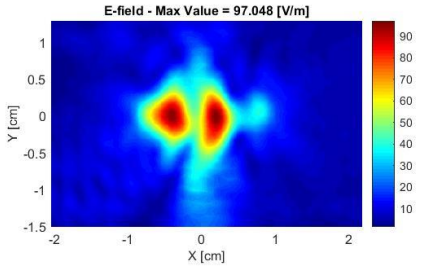	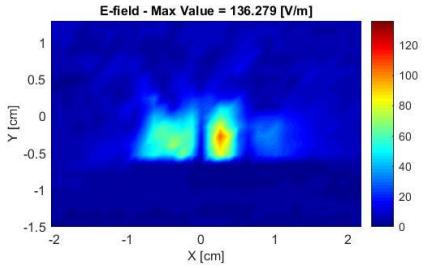
E-field (V/m) @ 2 mm – Deviation of Max Value: 2.949 dB	
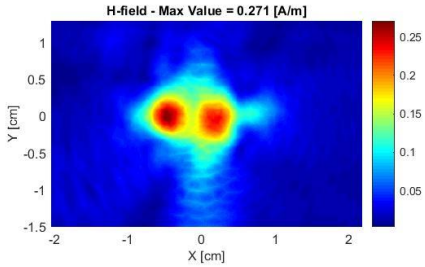	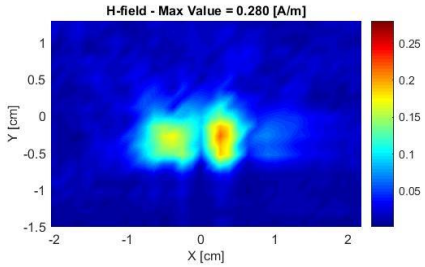
H-field (V/m) @ 2 mm – Deviation of Max Value: 0.308 dB	
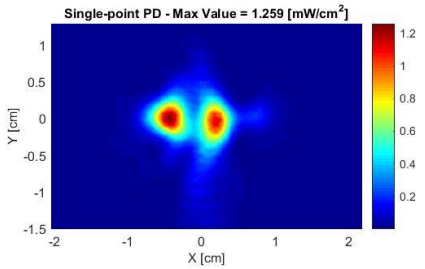	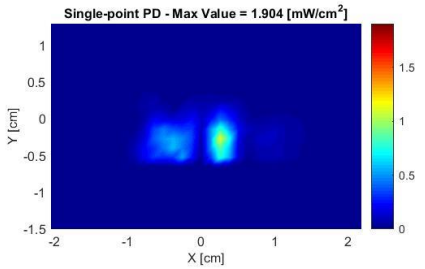
Localized free space PD (mW/cm2) @ 2 mm – Deviation of Max Value: 1.794 dB	
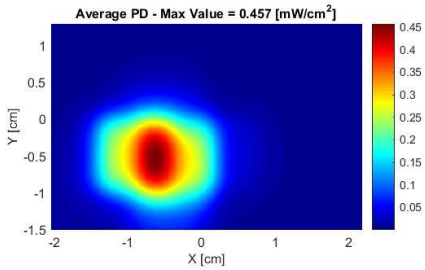	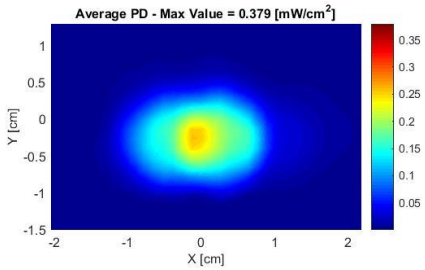
Spatially Averaged PD (mW/cm2) @ 2 mm – Deviation of Max Value: 0.812 dB	

Case #2 - DISTANCE = 5 mm	
Simulated	**Measured**
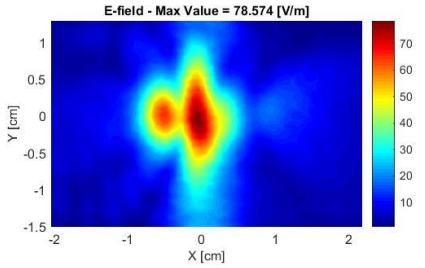	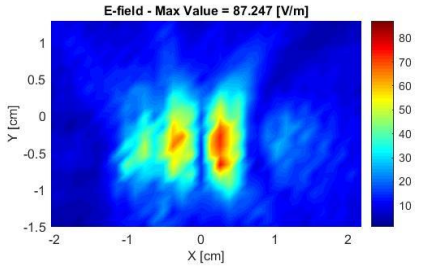
E-field (V/m) @ 5 mm – Deviation of Max Value: 0.909 dB	
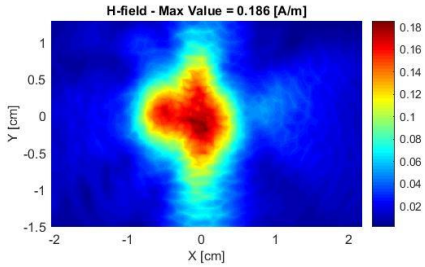	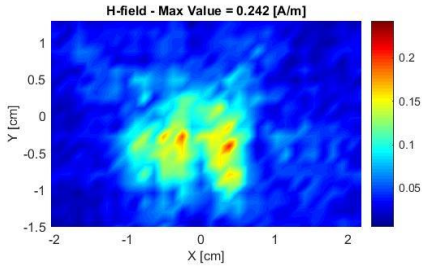
H-field (V/m) @ 5 mm – Deviation of Max Value: 2.323 dB	
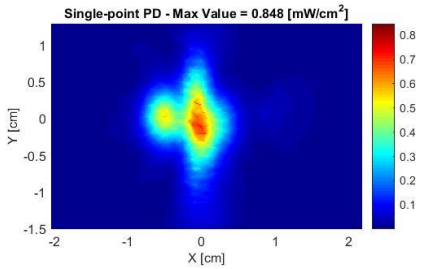	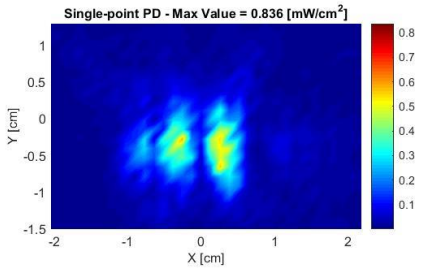
Localized free space PD (mW/cm2) @ 5 mm – Deviation of Max Value: 0.060 dB	
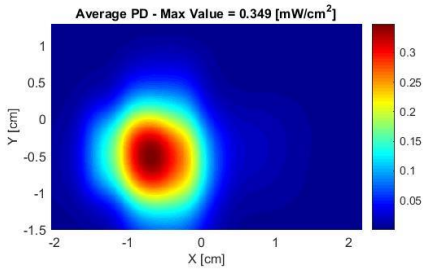	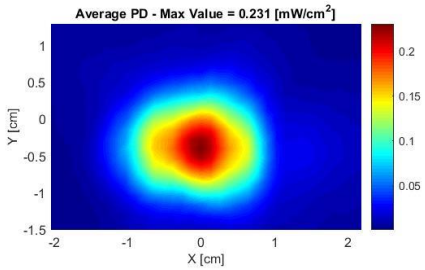
Spatially Averaged PD (mW/cm2) @ 5 mm – Deviation of Max Value: 1.796 dB	

Case #4 - DISTANCE = 2 mm	
Simulated	**Measured**
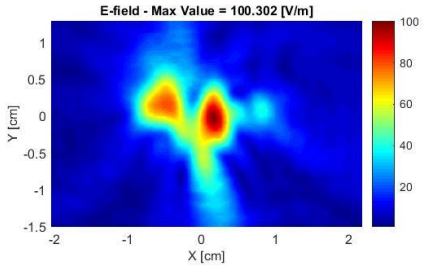	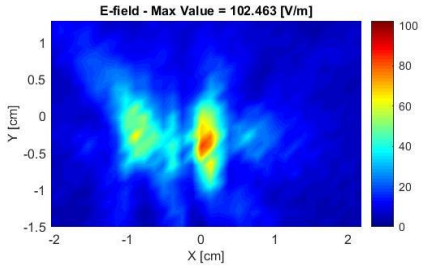
E-field (V/m) @ 2 mm – Deviation of Max Value: 0.185 dB	
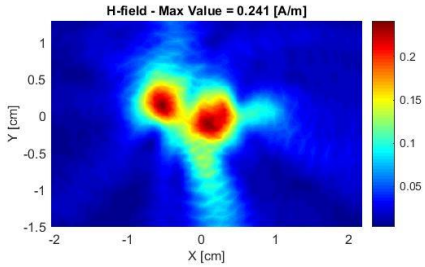	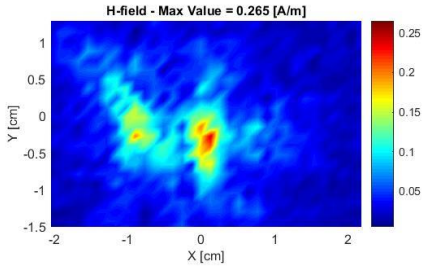
H-field (V/m) @ 2 mm – Deviation of Max Value: 0.814 dB	
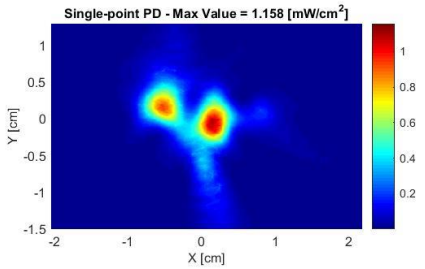	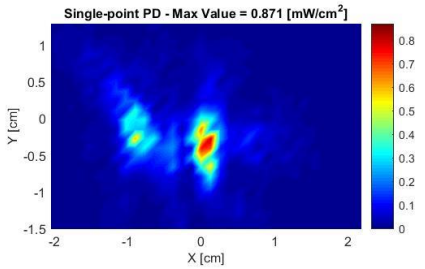
Localized free space PD (mW/cm2) @ 2 mm – Deviation of Max Value: 1.233 dB	
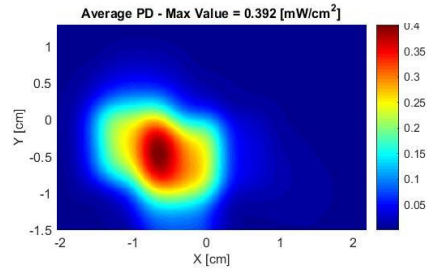	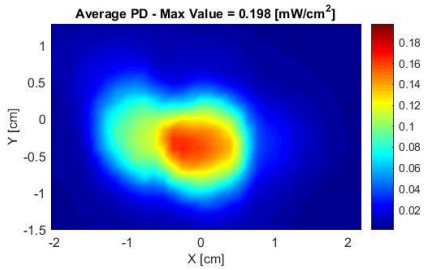
Spatially Averaged PD (mW/cm2) @ 2 mm – Deviation of Max Value: 2.970 dB	

Case #4 - DISTANCE = 5 mm	
Simulated	**Measured**
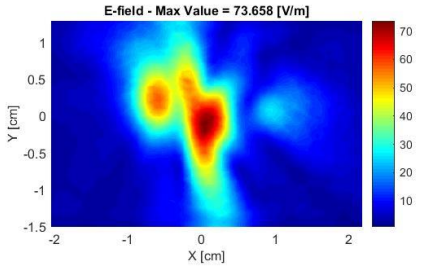	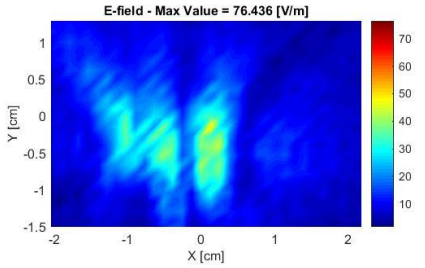
E-field (V/m) @ 5 mm – Deviation of Max Value: 0.322 dB	
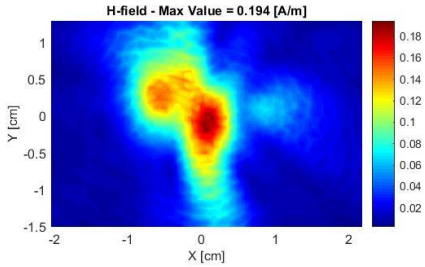	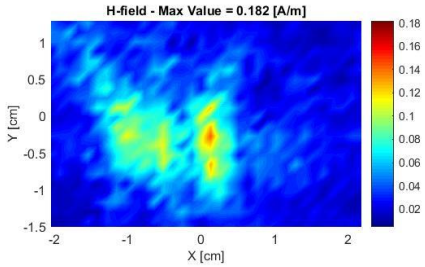
H-field (V/m) @ 5 mm – Deviation of Max Value: 0.585 dB	
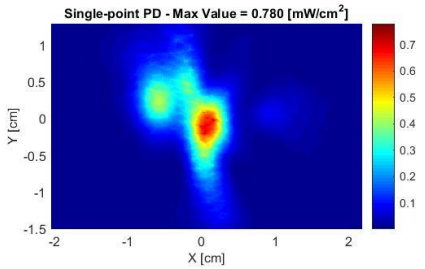	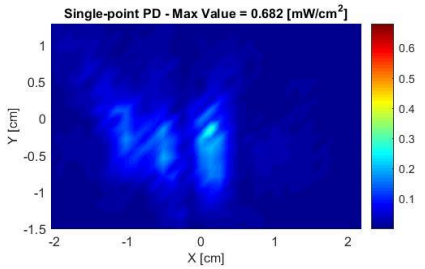
Localized free space PD (mW/cm2) @ 5 mm – Deviation of Max Value: 0.584 dB	
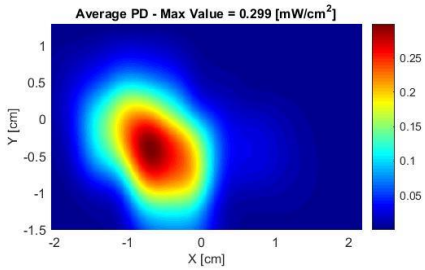	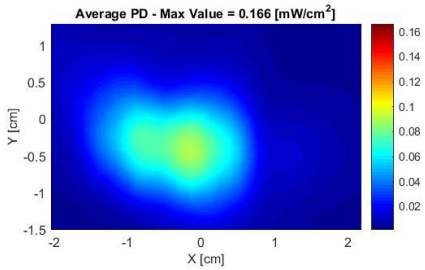
Spatially Averaged PD (mW/cm2) @ 5 mm – Deviation of Max Value: 2.548 dB	

B.6 Conclusion

The near field measurement shows a good correlation with the near field simulation with a maximum deviation below 3 dB for the measured distances.